Published in final edited form as:
Plasmonics. 2006 March 1; 1(1): 5–33. doi:10.1007/s11468-005-9002-3.

Plasmonics in Biology and Plasmon-Controlled Fluorescence

Joseph R. Lakowicz
Center for Fluorescence Spectroscopy, Department of Biochemistry and Molecular Biology, University of Maryland at Baltimore, 725 West Lombard Street, Baltimore, MD 21201, USA

Abstract

Fluorescence technology is fully entrenched in all aspects of biological research. To a significant extent, future advances in biology and medicine depend on the advances in the capabilities of fluorescence measurements. As examples, the sensitivity of many clinical assays is limited by sample autofluorescence, single-molecule detection is limited by the brightness and photostability of the fluorophores, and the spatial resolution of cellular imaging is limited to about one-half of the wavelength of the incident light. We believe a combination of fluorescence, plasmonics, and nanofabrication can fundamentally change and increase the capabilities of fluorescence technology. Surface plasmons are collective oscillations of free electrons in metallic surfaces and particles. Surface plasmons, without fluorescence, are already in use to a limited extent in biological research. These applications include the use of surface plasmon resonance to measure bioaffinity reactions and the use of metal colloids as light-scattering probes. However, the uses of surface plasmons in biology are not limited to their optical absorption or extinction. We now know that fluorophores in the excited state can create plasmons that radiate into the far field and that fluorophores in the ground state can interact with and be excited by surface plasmons. These reciprocal interactions suggest that the novel optical absorption and scattering properties of metallic nanostructures can be used to control the decay rates, location, and direction of fluorophore emission. We refer to these phenomena as plasmon-controlled fluorescence (PCF). We predict that PCF will result in a new generation of probes and devices. These likely possibilities include ultrabright single-particle probes that do not photobleach, probes for selective multiphoton excitation with decreased light intensities, and distance measurements in biomolecular assemblies in the range from 10 to 200 nm. Additionally, PCF is likely to allow design of structures that enhance emission at specific wavelengths and the creation of new devices that control and transport the energy from excited fluorophores in the form of plasmons, and then convert the plasmons back to light. Finally, it appears possible that the use of PCF will allow construction of wide-field optical microscopy with subwavelength spatial resolution down to 25 nm.

Keywords

Plasmonics; Fluorescence; Surface plasmons; Radiative decay engineering; Metal-enhanced fluorescence; Nanotechnology; Nanofabrication; Time-resolved fluorescence

Introduction to plasmon-controlled fluorescence

Fluorescence detection is the basis of many measurements in biological research. The principles and applications of fluorescence have undergone extensive development since its introduction to biochemistry in the 1950s. Fluorescence provides numerous measurement opportunities including studies of biological macromolecules, cell imaging, and DNA

lakowicz@umbi.umb.edu.

sequencing. Exotic phenomena such as multiphoton excitation and time-resolved microscopy are now routinely performed in many laboratories for cellular imaging. In our opinion, fluorescence technology has reached a plateau in which the fundamental principles are mostly developed. Most advances in fluorescence are now accomplished within the framework of specific applications, such as the development of red and near-infrared (NIR) probes for animal imaging, the development of molecular beacons for DNA and RNA detection, and the development of genetically engineered probes such as the green fluorescent protein (GFP), which can be expressed in living cells and even whole organisms.

We believe that fluorescence is now poised for a paradigm shift that will change the ways we think about fluorescence and will expand its experimental capabilities. At present, essentially all uses of fluorescence depend on the spontaneous emission of photons occurring nearly isotopically in all directions (Figure 1). Information about the samples is obtained mostly from changes in the nonradiative decay rates, such as collisions of fluorophores with quenchers and fluorescence resonance energy transfer (FRET). The rates of spontaneous emission are not significantly changed in such experiments. The only way to significantly change the spontaneous decay rates is to change the fluorophore, such as the use of the long-lived lanthanides, the use of transition metal-ligand complexes, or the use of phosphorescence. At present, the timescale and spatial distribution of fluorescence are not controlled by the experimental conditions.

In recent papers, we began to consider methods to modify the radiative decay rates of fluorophores [1,2]. From a review of the literature, we found that radiative decay rates could be modified by proximity of fluorophores to metallic particles such as silver colloids. We use the term metal to describe conducting metallic surfaces and particles, not metal ions. The effects of metals on fluorescence have been subject to prior theoretical reports [3-6], but the practical usefulness of these effects was not explicitly recognized. We refer to the interactions of fluorophores with novel metal particles as radiative decay engineering (RDE) because the radiative decay rates of the fluorophores are modified by placing the fluorophores in close proximity to the metal [7,8]. We observed a variety of favorable effects due to metal particles, such as increased fluorescence intensities, increased photostability, and increased distances for FRET. We refer to these favorable effects as metal-enhanced fluorescence (MEF).

Our studies of the interactions of fluorophores with metal particles led to studies of fluorophores near planar metallic surfaces. The metal surfaces were similar to those used for surface plasmon resonance (SPR), which is a continuous surface of silver or gold about 40 nm thick on a glass substrate. These thin metal films are visually nearly opaque. We found that excitation of fluorophores near these surfaces resulted in strong directional emission into the substrate. The emission appeared as a cone with a half-angle consistent with the SPR angle for the emission wavelength, and there was little emission into the air away from the glass substrate [9,10]. The emission spectra were found to precisely match the emission spectra of the fluorophore, so it was not clear if the fluorophore or the plasmon was responsible for the observed emission. Other groups made similar observations [11-13], some dating back to 1975 [14], but in these papers it is often unclear if the emission is attributed to the fluorophore or the plasmons. We refer to this unusual phenomenon as surface plasmon-coupled emission (SPCE). This name is appropriate because the directional emission was subsequently shown to be due to plasmons created by the excited fluorophores and not due to creation of plasmons by the incident light [15].

The observations of MEF and SPCE led to our vision for plasmon-controlled fluorescence (PCF). As shown schematically in Figure 2, the interaction of fluorophores with metals can affect both excitation and emission. Effects on excitation are possible because the electric fields from the incident light can be concentrated in small metallic colloids. Additionally,

fluorophores near metal colloids can show increased rates of radiative decay Γ in the absence of metal particles. Finally, the emission can occur in defined directions by the use of metallic nanostructures. In our opinion, these effects will result in a new generation of devices in which the emission energy is controlled by metallic nanostructures.

Mechanism of plasmon-controlled fluorescence

The observation of SPCE showed that excited-state fluorophores could undergo near-field interactions with the metal surface to create surface plasmons, which in turn radiate into the substrate. It was surprising that excited fluorophores could create plasmons because it is well known that light incident on the metal, from the same side as the fluorophore, cannot create surface plasmons. The complete p-polarization of the SPCE indicated that the plasmons were responsible for the far-field radiation propagating in the substrate. The ability of excited-state fluorophores to create plasmons opens the possibility of using plasmonic structures to manipulate fluorescence.

The experiments with metal particles and surfaces caused us to question what optical and/or geometric properties of the system were responsible for the useful interactions of fluorophores with metals. We developed a relatively simple concept that MEF was the result of surface plasmons that were capable of creating far-field radiation [16]. This seemingly simple concept was hidden from us by the complex language of surface plasmons and light scattering. As an illustration, Mie theory shows that the extinction of metal particles is due to two effects: light absorption and light scattering [17,18]. The combination of scattering and absorption is called the extinction. Based on the language of fluorescence, scattered light is a problem to be eliminated. However, in the language of Mie theory, the scattering component represents the ability of a particle to radiate into the far field. That is, the incident light induces electron oscillations in the metal. These oscillations act like dipoles that can radiate light. Hence, the scattering component of the cross section of metallic colloids is analogous to fluorescence. The ability of plasmons to radiate can be understood, at least at a superficial level, by consideration of wave vector matching at the interface of the metal with its surrounding environment. The concept of wave vector matching at interfaces is fundamental to optics and electrodynamics [19,20]. Light cannot cross an interface unless wave vector matching occurs at the interface. Wave vectors matching at an interface is equivalent to having a continuous electric field across the interface. In Mie theory, the absorption component of the optical cross section of a colloid is due to plasmons that cannot radiate and thus the energy is dissipated as heat. The scattering component of the optical cross section is due to radiation from the induced plasmons.

We believe that the scattering component of metal particle extinction is responsible for enhanced fluorescence because the fluorophore-induced plasmons can radiate, and that this radiative decay occurs more rapidly than in the absence of metal. This model for MEF assumes that the fluorescence wavelengths are longer than the interband transitions of the metal. MEF is expected to occur when the absorption and/or emission bands of the fluorophore overlap with the scattering wavelength of the metal structure. We refer to this concept as the radiating plasmon (RP) model. This model is supported by some preliminary experiments, which showed larger fluorescence enhancements with particles or particle aggregates displaying longer wavelength extinction [21-24], which is usually due to scattering more than absorption. To our knowledge, the RP model has not been conclusively proven, but the reasonableness of the model has resulted in its general acceptance.

The RP model provides a rational link between fluorescence and the emerging science of surface plasmons, which is now called “plasmonics.” The wavelengths of plasmons can be considerably shorter than the incident wavelengths. As a result, the study of surface plasmons has become of great interest for nano-optics, nanolithography, and for the next generation of

computer chips that utilize subwavelength size structures [25-27]. At first glance, it appears that experimentation with plasmons is not necessary and that everything can be calculated using Maxwell's equations. However, many optical effects due to plasmons were not anticipated from classical electrodynamics. One example is the Wood's anomaly with optical gratings, which was first described in 1935 [28,29]. At that time, it was found that metallic gratings did not reflect light at specific wavelengths and polarizations. The origin of this effect was not known. It is now known that this effect is due to the strong absorption by surface plasmons that are created by the incident light interacting with the metal film and the periodic structure of the grating. Another example is the transmission efficiency of subwavelength apertures. For an opaque dielectric material, the transmission efficiency becomes very low when the aperture is smaller than the optical wavelength, and the transmitted light is fully diffracted into the half space. However, in 1998 it was discovered that arrays of subwavelength nanoholes in opaque metal films display anomalously high optical transmission that can be orders of magnitude larger than the relative areas of the holes and metal surface [30]. The light transmitted by a nanohole in a metal film is not necessarily diffracted into half-space, but can beam with a small angular divergence [31]. Whereas these phenomena must be contained within Maxwell's equations, they were not known prior to the experimental observations. The optical properties of metallic nanostructures were not anticipated from classical electrodynamics because analytical solutions of Maxwell's equations are limited to relatively simple symmetric structures. However, with modern computers electrodynamic calculations have become routine for complex macroscopic objects [32,33]. These computational methods can also be used to simulate anomalous transmission and beaming transmission [30,31], but in this case, the observations preceded the simulations. Unfortunately, the calculations may not be completely reliable for metallic nanostructures and near-field effects. The optical properties of these structures may differ from that of the bulk metals. Additionally, numerical solutions of Maxwell's equations may not provide physical insight into the phenomena. As a result, determination of the optical properties of metallic nanostructures is typically a combination of theory, simulations, and experimentation. The combination of plasmonics with fluorescence may be even more complex because of the finite size and asymmetry of most fluorophores, specific chemical effects, and failure of the point-dipole model for fluorophores at small distances from the metal surface.

The field of plasmonics will expand to include much more than SPR and anomalous transmission. Surface plasmons are of interest because they can have wavelengths much smaller than optical wavelengths, suggesting their use for subwavelength lithography, optical computing and imaging. Surface plasmons can be engineered to either radiate or remain trapped at the metal surface. The ability of fluorophores to respond to and/or create surface plasmons suggests the combination of plasmonics and fluorescence for the next generation of fluorescence technology.

Opportunities for plasmonics in biological fluorescence

The combined use of plasmonic structures and fluorescence is in its infancy, but we see considerable potential for new capabilities in fluorescence technology. It would be impossible to predict all the future developments in this area of research. However, it seems valuable to suggest some of the future possibilities. Based on our current understanding, we believe the rational use of fluorophore-plasmon interactions can result in a number of new research capabilities. These possibilities include:

1. Ultrabright probes, which are 1000-fold brighter than currently available fluorophores and which can be monitored indefinitely at the single-particle level without photobleaching.

2. The ability to measure distances between biomolecules in the presently inaccessible distance range from the 10-nm FRET limit up to 200 nm.
3. Probes that provide localized multiphoton excitation with low-intensity wide-field illumination.
4. Metallic structures that selectively enhance excitation or emission at desired wavelengths without enhancing background emission at other wavelengths.
5. New diagnosis devices based on PCF and energy transport.
6. Wide-field subwavelength optical microscopy. One can already imagine schemes whereby 30-nm spatial resolution can be obtained using wide-field methods. The availability of such microscopy would revolutionize cell biology and imaging.

In the following sections we will describe how these capabilities can be obtained based on information available in the plasmonics literature and the known ability of excited fluorophores to induce radiating plasmons.

Current applications of plasmonics in biology

The phenomenon of surface plasmon resonance (SPR) is widely used to measure binding interactions between biomolecules [34,35]. SPR is accomplished by illuminating a thin metal film, typically 40 nm gold, through a glass prism (Figure 3, top). The light is reflected from the film at all angles except for a narrow range of angles where the film absorbs the light. This absorption is not due to any chromophores, but rather to resonant electron oscillations induced in the film by the incident light (Figure 3, bottom). Resonant absorption occurs at the metal-sample interface when the in-plane wave vector (k_X) of the incident light matches the wave vector of the surface plasmons k_{sp}. The surface plasmon wave vector is determined by the incident free-space wave vector k_0 and thedielectric constants of the metal film (ε_m) and of the sample (ε_s) according to [36-38]

$$k_{sp}=\frac{\omega}{c}\left(\frac{\varepsilon_m\varepsilon_s}{\varepsilon_m+\varepsilon_s}\right)^{1/2}=k_0\left(\frac{\varepsilon_m\varepsilon_s}{\varepsilon_m+\varepsilon_s}\right)^{1/2} \quad (1)$$

Somewhat surprisingly, the surface plasmon wave vector is not affected by the refractive index of the prism, but the refractive index of the prism affects the incidence angle where the surface plasmon resonance occurs. The optical properties of metals are complex to understand. The dielectric constants of metals are usually described by complex numbers so that

$$\varepsilon_m=\varepsilon_r+i\varepsilon_{im} \quad (2)$$

where ε_r is the real part and ε_{im} is the imaginary component (Figure 4). The real part of the dielectric constant is related to the conductivity of the metal and is typically negative above the plasmon frequency. The real part of the dielectric constant is also related to the penetration depth of the electric field in the metal. The electric and magnetic fields are strongly attenuated in the metal [36]. For example, at 600 nm the distance for 1/*e* attenuation are 24 nm for silver and 31 nm for gold (Figure 5).

In order to obtain resonance, the in-plane (xy plane) wave vector of the incident light must equal the surface plasmon wave vector. Because the real part of ε_m is often much larger than the imaginary part, the wave vector for the plasmons can be approximated by

$$k_{sp}=k_0\left(\frac{\varepsilon_r\varepsilon_s}{\varepsilon_r+\varepsilon_s}\right)^{1/2} \tag{3}$$

The incident light can excite a surface plasmon when its *x* axis component equals the wave vector for the surface plasmon. The wave vector for the incident light in the prism (*p*) is given by

$$k_p=k_0 n_p \tag{4}$$

where n_p is the refractive index of the prism. This value is related to the dielectric constant of the prism ε_p by $n_p = \sqrt{\varepsilon_p}$. The conditions for SPR absorption are satisfied when

$$k_{sp}=k_x=k_0 n_p \sin\theta_{sp} \tag{5}$$

where θ_{sp} is the angle measured from the normal where absorption occurs. Surface plasmon resonance occurs whenever the angle of incidence results in a component that equals that obtained from Eq. (3).

It is interesting to note that the SPR angle is sensitive to the dielectric constant of the sample. This is because the resonance occurs at the metal-sample interface. The incident light is adsorbed but the plasmons cannot radiate into the sample because their wave vectors are larger than the wave vectors for light of the same frequency in the sample. As a result, there is an evanescent field that extends a fraction of wavelength into the sample. The sensitivity of the SPR angle to biomolecule binding at this surface is due to interactions of the evanescent field with the sample adjacent to the metal surface. SPR does not involve chromophores in the biomolecules because the interaction is due changes in the refractive index to $n_s = \sqrt{\varepsilon_s}$ near the film due to biomolecule binding.

Another current application of plasmonics in biology is the use of metallic colloids as probes. Suspensions of metallic colloids display brilliant colors that result from both absorption and scattering of light [39,40]. The colors of colloids are not due to chromophores but rather to electron oscillations in the colloids induced by the incident light (Figure 6). The energy contained in these oscillations is dissipated by dipole radiation into the far field and by conversion into heat. These mechanisms account for the absorption and scattering components of the colloid extinction. The electron oscillation in colloids is also called plasmons. These plasmons are the same phenomenon that occurs in SPR, except that the plasmons are constrained by the size of the colloid. It is much easier to induce plasmons in colloids than in continuous metal film. For continuous films, it is necessary to use a prism and precise angle of incidence to match the plasmon resonance. No special conditions are needed to excite plasmons in colloids. Incident light interacts with colloids irrespective of the surrounding environment.

There have been numerous papers and monographs on the optical properties of metal colloids, which are often described using Mie theory. This theory is relatively simple for subwavelength size spheres. In this case, the cross sections for extinction C_E is given by

$$C_E=C_A+C_S=k_1 \mathrm{Im}\,(\alpha)+\frac{k_1^4}{6\pi}|\alpha|^2, \tag{6}$$

where $k_1 = 2\pi n_1/\lambda_0$ is the wave vector of the incident light in medium 1 and a is the polarizability of the sphere of radius r

$$\alpha = 4\pi r^3 \left(\frac{\varepsilon_m - \varepsilon_1}{\varepsilon_m + 2\varepsilon_1} \right), \tag{7}$$

The term $|\alpha|^2$ is the square of the modulus of α, C_A is the cross section due to absorption, and C_S is the cross section due to scattering. When discussing the cross sections of colloids it is convenient to use the efficiencies (Q) for extinction (E), absorption (A) and scattering (S), Q_E, Q_A, and Q_S, respectively [41]. These values are obtained by dividing the cross sections for interaction with light by the geometric cross sections πr^2. These efficiencies represent the ability of the particle to scatter light relative to its physical cross-sectional area.

Incident light interacts very strongly with metallic colloids [40]. This property is shown in Figure 7 where a colloid is illuminated with light (λ) with a wavelength that matches the plasmon resonance at λ_P (top) or with a wavelength longer than λ_P (bottom). The lines show the energy flow near the particle. For a resonant wavelength, the colloid can have an optical cross section much greater than its physical cross section. This effect is seen by the energy flow into the particle, which results in the enhanced fields near illuminated colloids. For a nonresonant wavelength, the optical cross section can be similar to or smaller than the physical cross section (bottom), which is typical of organic fluorophores and semiconductor nanoparticles also known as quantum dots (Qdots). A useful descriptive name for metallic colloids is plasmon resonance particles (PRPs) [42], which accurately describes their optical properties.

Recent applications of SPR and PRPs

The previous section described the properties of plasmons occurring on a smooth metal film and the spatially limited oscillations that take place in metallic colloids or PRPs. These two types of plasmons are already finding applications in biomedical assays and imaging. Some simple assays take advantage of the high optical cross sections of the colloids, which makes low concentration of colloids visible to the naked eye. One example is shown in Figure 8, which shows the structure of a DNA oligomer (CS-DNA) labeled on both ends with core-shell (CS) particles [43]. Hybridization of the CS-DNA with the target can be seen simply by spotting the solution onto a thin-layer plate (lower left). The unhybridized DNA is seen as a yellow spot and the hybridized CS-DNA is seen as a brown spot. The changes in color are due to interactions between the particles on each end of the oligomer, which depend on the distance between the particles. Increasing the temperature above the melting temperature T_m dissociates the strands and reverses the color change. Small changes in the chemical composition of the particle can yield different colors. For gold particles, the color change is from purple to brown/black upon hybridization (lower right). These spots are easily visible to the naked eye because of the high extinction cross sections of the colloids.

Another example of DNA hybridization detected using plasmonic particles is shown in Figure 9. In this case, the particles were gold colloids. Separate samples of these colloids were labeled with one of two DNA oligomers (a or b). These oligomers (a and b) were not complementary. The target DNA (a'b') was complementary to both oligomers. Addition of the target DNA (a'b') causes the colloids to form aggregates. The interactions between the gold particles in the aggregates change the extinction spectra, and color change can be seen visually. The color changes are due to through-space interactions between the colloids. A through-space interaction is somewhat predictable in that it is not dependent on the specific chemistry or type

of biomolecule. The through-space interactions between colloids typically occur over a distance of 2.5 times the diameter of the particles.

Single molecule detection (SMD) is often described as the ultimate in sensitivity. However, SMD is usually accomplished under specialized conditions to restrict the observation volume to a small region around the molecule [45]. As currently practiced, SMD is not a method for high-sensitivity assays. Single molecules can be observed but are not easily counted. The high optical cross of individual metal colloids or PRPs allow them to be visualized without any special conditions [46]. Figure 10 shows a photograph of three PRPs taken with a white light epi-illumination microscope without additional filters. The three different size colloids are easily visible from the light scattering at different wavelengths (top). It is even possible to measure the scattering spectra of the individual particles (bottom). It would not be possible to visualize individual fluorophores using these same conditions. SMD of fluorophores is accomplished with extensive filtering and attention to the overall optical efficiency. The PRPs in Figure 10 were observed with a wide-field microscope and epi-illumination. Single PRPs have also been observed in bacterial cells [47]. Gold particles have been used to track receptors on cervical cancer cells using reflected light [48]. The ability to easily detect single PRPs is due to their large optical cross sections (Figure 9) and high quantum efficiency for light scattering [41].

In SMD background fluorescence can easily obscure the signal from single fluorophores. Remarkably, PRPs can be observed in the presence of high background fluorescence. Figure 11 shows a photograph of a *Drosophila* polytene chromosome [46] The green color is due to SYBR Green, which was used to stain the nucleic acids. The bright spots are due to single PRPs that were directed to specific sites on the chromosome using in situ hybridization. Single PRPs can be seen even with the high background due to SYBR Green. It is highly unlikely that single fluorophores or single Qdots could be observed under similar conditions.

The previous examples used continuous metal surfaces (SPR) or particles (PRPs). Reports are now appearing that combine both types of metallic structures. One example uses metal colloids to increase the sensitivity of SPR [49-51]. The usual SPR binding assays are performed using unlabeled biomolecules. The changes in SPR angle are usually small, about 0.1°, because the refractive of the solution index above the metal film is only slightly changed by the bound molecules. The changes in angle can be increased many fold by the use of biomolecules that are conjugated to metal colloids. In this case there is a larger change in the effective dielectric constant near the metal film because the dielectric constant of the PRPs is very different from that of water, the amount of bound mass is larger, and the particles and metal surfaces interact through space over distances up to about 100 nm.

An example of the increased sensitivity of SPR using metal colloids is shown in Figure 12 [51]. In this case, a capture DNA oligomer1 (S1) was bound to the gold surface. Binding of a complementary oligomer S2 had only a minor effect on the angle-dependent reflectance, shifting the reflectance minimum by 0.1°. Binding of the oligomer containing the gold particle resulted in a shift of 1.8°, an 18-fold increase. This result shows that the interactions between metallic particles and surfaces can be used to increase the delectability of bioaffinity reactions.

The use of PRPs in cell imaging and metal colloids in SPR can be regarded as early examples of plasmonics in biology. In these cases, the interaction between metallic structures is being used to obtain biochemical information about the system. The optical changes are large because of the strong interactions of light with the metals. We believe that the strong interactions between fluorophores and surface plasmons will also be used to study a wide range of biological phenomena.

Plasmonics and fluorescence

In the previous section we described the present uses of metallic structures for biochemical analysis and imaging. We believe these examples represent only the beginning of the use of plasmonic structures in biology. The previous examples relied on the interaction of light with the metallic structures, followed by detection of the light at the same wavelength that is reflected or scattered from the structures. These uses of plasmonics, although powerful, lack the advantage of a Stokes' shift. We believe it will be possible to maintain some of the properties of plasmons (strong interactions with light) with the spectral characteristics of fluorescence (Stokes shift, time-delayed emission, etc.). This will be possible because the near fields created by plasmon resonances can interact with fluorophores and serve as a source of local fields and amplified excitation. Additionally, excited fluorophores can undergo near-field interactions with metals, creating plasmons that are then radiated into free space.

The concept of using plasmonic structures to control fluorescence is shown in Figure 13. In such a device, the fluorophores would be in close proximity to a silver surface and the silver surface will have a defined nanostructure. For example, the two regions on the left could contain nanohole arrays. The spacing of the nanoholes could be chosen for anomalous transmission of green (G) or red (R) wavelengths. The fluorophores with green or red emission will preferentially couple to plasmons in the respective structures. We expect the plasmons will then radiate into the substrate for detection. Alternatively, the surface on the right can be patterned as a thin metal grating. In this case, both the green and red fluorophores will couple to the surface, but the green and red emission will appear at different angles in the substrate.

Ultrabright fluorescent particles

Plasmonic structures can also be used to obtain increased fluorescence intensities or to obtain ultrabright particles. This application of PCF will depend on the use of metallic particles with varying sizes and shapes. For instance, consider a fluorophore contained within a metallic nanoshell, as compared with a fluorophore in solution (Figure 14). In the absence of a metal particle, the fluorophore feels the incident light field (E) at the excitation wavelength (λ_{ex}) and emits with the usual radiative decay rate Γ at the emission wavelength λ_{em}. The extent of absorption is determined by the optical cross section of the fluorophore, which is usually a fraction of its physical cross section. Now consider a fluorophore within a silver shell and assume that light absorbed by the metal shell is transferred to the fluorophore. The effective cross section for absorption is now much larger than that of the fluorophore, and even larger than the colloid itself. This effect results in a higher effective incident field E_m at the excitation wavelength and increased excitation of the fluorophore due to the amplified incident field. For the moment, we are assuming the silver shell does not transform any of the energy into heat. As described in the introduction, fluorophores near metals can have higher radiative decay rates and higher quantum yields than in the absence of metals. Hence, the emission intensity of the fluorophore in the metal shell can be increased further by the ability of the fluorophore to induce plasmons in the shell, which in turn radiate as light. These considerations suggest a fluorophore in a nanoshell, or other suitable structures can have the useful Stokes' shift of fluorescence with the high optical cross section of a PRP.

In describing a fluorophore in a nanoshell we described the excitation and emission in terms of wavelength. In the case of absorption and fluorescence in the absence of metals, this convention is convenient because the wavelengths are changed to only a modest extent by the sample. In the case of metals, it is important to remember that the energy of the light is described unambiguously by its frequency. The energy at a given frequency can be contained in a plasmonic structure or a nanoshell that has dimensions much smaller than the free-space wavelength for this same frequency.

The potential of plasmonics for creating ultrabright fluorescent particles is best shown by specific examples. We believe it will be possible to create ultrabright and photostable probes by combining fluorophores with metal particles. At this time, it is not clear if the brightest probes will be obtained for fluorophores on particles or inside of shell particles. The optimal size and shape of the particle(s) for maximal brightness is also unknown. It is difficult to calculate the optical properties of any metallic shape other than a sphere (Table 1). These less symmetrical shapes usually require numerical methods. An additional level of complexity arises when a fluorophore is placed very close to the metal, where there will be effects due to the chemical structure, orientation, and other unknown factors. Calculations have been reported for one simple geometry, rhodamine 6G (R6G) in a silver nanoshell (Figure 15). This system has been the subject of electrodynamics calculations [52,53]. These calculations included the loss of energy as heat during transfer of energy across the silver shell in both directions and should thus provide a reliable estimate of the emission intensity. Even after this attenuation, the emission from a single fluorophore is expected to be 10- to 100-fold higher when contained in a nanoshell. At this time, we do not know if there are other factors that may make the fluorophore less bright, but this is nonetheless a promising result.

There are other factors that can result in larger enhancements than shown in Figure 16. The shorter lifetime of the fluorophore results in less time for photochemistry while in the excited state, and thus more excitation-emission cycles prior to photobleaching. The metal shell may be impermeable to oxygen and other species that react with the fluorophore and thus protect the fluorophore from photochemical reactions. There is no reason to limit the nanoshell to contain a single fluorophore. We have already shown that proximity to metallic particles decreases self-quenching due to homo FRET [54] so that tens of fluorophores can be placed within the nanoshell. It is known that the electric fields within these shells is uniform [55], suggesting that all the fluorophores may be equally enhanced irrespective of location within the nanoshell. These considerations suggest that fluorophores encapsulated in metal nanoshells can be bright and photostable particles for single-molecule detection and imaging.

It is informative to compare a fluorophore in a nanoshell, which we will call a plasmonic probe, with semiconductor nanoparticles or Qdots. Since Qdots are already in use for cellular and whole-animal imaging [56-60], one can expect the plasmonic fluorophores to be used in similar applications. Qdots are frequently targeted to internal or external regions of cells using specific antibodies or peptides. Similar surface chemistries can be used to attach proteins to the surfaces of metal particles. This surface labeling of metal particles may be even easier with silver and gold particles because of the intrinsic affinity of these metals for amino and sulfhydryl groups. The Qdots have been found very useful even though their brightness is comparable to a single fluorophore or a few fluorophores. The Qdots contain materials such as CdS or CdSe, which can be toxic to cells under some conditions [61]. Impermeable surface coatings are often required to prevent leakage of the toxic materials. In contrast to Qdots, silver and gold are essentially nontoxic and, if needed, can also be coated with silica or biocompatible materials. The Qdots are claimed to be highly photostable. This is a result of the surface coating since uncoated semiconductor Qdots are sensitive to the local environment and undergo photobleaching. Similarly, the silver coating over the fluorophore is likely to result in increased photostability. We expect the plasmonic probes to be easily 100-fold brighter than a single fluorophore and thus as useful as Qdots.

An advantage of Qdots is their ability to be excited at any wavelength and their narrow emission spectra [62,63]. These same advantages are expected for plasmonic probes. Gold and silver nanoshells are known to display broad absorption [64,65]. We expect the excitation spectra of plasmonic probes to be comparable to broad absorption of the nanoshells. Quantum dots are known to display narrow emission spectra. Fluorophores within metal shells are also expected to display more narrow emission spectra without the long-wavelength tails [52,53]. In fact, the

calculated emission spectrum for rhodamine 6G in a silver shell is about 2-fold more narrow than in solution (Figure 15). In summary, plasmonic probes are potentially brighter, more photostable, and less toxic than Qdots.

Subwavelength distance measurements

Two ranges of distances are readily available in live cell imaging. Distances ranging from macroscopic to about $\lambda/2$, typically 300 nm, are measurable using confocal, multiphoton, and/or laser scanning methods [66,67]. A shorter range of molecular size distances are available using FRET, which occurs over distances ranging from 1 to 10 nm. Distances measurable by FRET are usually less than 6 nm. The extent of FRET can be imaged in a microscope, providing an image of proximity between donor and acceptor labeled biomolecules. The individual biomolecules are usually not imaged, and only the average donor-acceptor proximity is contained in the FRET image [68,69]. However, far-field optical microscopy does not allow distance measurements in the range from 10 to 300 nm. Near field methods are used for imaging from 10 to 300 nm, including near-field scanning optical microscopy (NSOM), atomic force microscopy (AFM), and scanning tunneling microscopy (STM). These methods rely on physically scanning the position of optical or mechanical probes over the region of interest, and are thus difficult to use for live cell imaging.

Many cellular processes and structures occur over a range of distances larger than FRET distances but smaller than optical resolution. Receptor proteins on cell membranes can form clusters that can be detected by FRET but are too small for optical imaging. Biomolecule assemblies often involves structures that are larger than FRET distances but below optical resolution. For example, FRET cannot be used to measure the distance across a ribosome because ribosomes have a diameter near 23 nm [70]. Complexation of antibodies with antigens is not always detectable using FRET because an IgG molecule is about 10 nm long and antigens can be even larger.

The existence of plasmons in metallic colloids provide an opportunity for measuring distances in the intermediate range from 10 to 300 nm. This possibility is the result of long-range coupling between metallic particles, which changes their optical properties. Figure 16 shows the calculated scattering spectra for two elliptical-shaped disks at various center-to-center distances. These calculations show that the scattering spectra are sensitive to distances ranging from about 50 to 150 nm [71]. The dependence of scattering on the distance between particles has been examined experimentally using samples prepared by nanofabrication. Figure 17 shows the electron micrograph and scattering spectra of individual pairs of silver disks on a substrate [72]. The scattering spectra are seen to be sensitive to edge-to-edge distances ranging from 10 to 250 nm. The scattering spectra are also sensitive to the polarization of the incident light, suggesting that different incident and observation polarizations can be used to gain additional information about the orientation of the particles. These results suggest that the scattering spectra of colloids can be used to measure distances in the range from 10 to 250 nm.

The use of colloid-colloid interactions for proximity imaging is shown in Figure 18. Each bright pixel in the word NANO is due to scattering of the white incident light by a pair of silver particles. The darker pixels contained only a single nanoparticle. The pairs of particles are easily identified from the higher intensities of the scattered light. The difference in color between the scattering particle pairs is due to variations in the exact dimensions of the pairs. Such variations should become less troublesome as nanolithographic methods improve or by the use of spherical colloids, which can be prepared with a high degree of homogeneity.

Cellular imaging experiments have already shown that scattering from colloids bound to cells can be sensitive to the distance between the colloids [73]. This application is based on the strong scattering power of metal colloids and on the effect of particle aggregation on the

intensity of the scattered light. Gold particles scatter light much more strongly than polystyrene particles (Figure 19). Additionally, clustering of the gold particle further increases the scattered intensity. This suggests that locations with clusters of colloids or clusters of biomolecules can be found from the location of higher scattering intensities.

The light scattered from colloids can be seen when the colloids are bound to cells. Figure 20 shows images of cancerous cervical cells that were labeled with colloids. The colloids were directed towards the epidermal growth factor receptor (EGFR) on the cell surfaces by binding antibodies to EGFR to the colloids [73]. The EGFR receptor is overexpressed in epithelial cancers. The cells were observed from the reflected light at 630-680 nm using a laser scanning confocal microscope (top). The bottom panel shows an overlay of the reflectance image and the transmission image. The scattered light from the colloids is easily visible even though there are only about 5000 copies of the EGFR per cell. Distances between the receptor were not measured in this experiment. However, the authors pointed out that they could not observe any scattered light from the colloids prior to their aggregation on the cell surfaces. Hence, the scattered intensity in Figure 20 is due to clustering of colloids.

The use of colloid-colloid interactions to measure distances is just beginning. In fact, the first use of these interactions to measure distances has just been published [74]. The possibility of distance measurements was tested using gold colloids linked by DNA oligomers (Figure 21). The gold colloids were highly charged and displayed electrostatic repulsion. The repulsion between the DNA-linked colloids was modified by changing the ionic strength of the solution. The peak scattering wavelength changed reversibly in response to ionic strength. The longer peak wavelength at higher ionic strength is consistent with increased interactions between more closely spaced colloids.

Calculation of the distances using scattering by colloids will require knowledge of the dependence of scattering on particle size, shape, distance, and polarization of the incident light. In the case of FRET, the dependence of transfer efficiency on distances is known and orientation effects are usually ignored. The rules for distance measurements using colloids are not yet known. It appears that the extent of interaction between colloids scales with the size of the colloids so that larger colloids can be used to measure larger distances. However, the spectral shifts can be complex, and smaller distances between particles sometimes result in blue shifts rather than the more commonly observed red shifts [75,76]. The observation of either blue or red shifts points to an underlying complexity of the particle-particle interactions, which must be understood before these interactions become widely used as a new type of molecular ruler. The present ability to use nanofabrication technology to create well-defined particle pairs suggests that we will be able to determine which interactions are important, and which can be ignored, as is presently known for FRET.

Nanostructures for enhanced wavelength-selective detection

In a previous section we described the possibility of ultrabright particles that would be detectable at the single particle level, even in the presence of background. We now consider the case where it is desirable to detect or count single fluorophores not coupled to metals, in the presence of background emission. Suppose the emission spectrum of the desired fluorophore occurs at 600 nm and the sample also displays autofluorescence from 400 to 800 nm. The fluorophore emission overlaps with the background and would be difficult to detect without some enhancement (Figure 22). Now suppose a plasmonic structure flow cell can be created that has a strong resonance at 600 nm. As described below, one such structure is an array of metal nanowires. Such a structure will increase the emission intensity of the 600-nm emission, without increasing the intensity of the autofluorescence at other wavelengths. Such wavelength-selective enhancement over a narrow range of wavelengths requires a plasmonic

structure that has a strong but narrow resonance. Of course, the autofluorescence at 600 nm would also be enhanced, but few natural substances have narrow emission spectra like modern fluorophores.

In recent years, several groups have calculated the optical properties of metallic nanorods and chains of particles [77-82]. Some of the calculations predict very narrow plasmon resonances. Figure 23 shows the calculated spectra for a chain of spherical silver nanoparticles, 200 nm in diameter, with the center-to-center spacing shown on the figure. The peak wavelength and width of the resonance depends on both particle size (not shown) and the spacing between the particles. The resonances can be very narrow. For example, the resonance at 800 nm is below 4 nm in width. The resonances are very strong as seen by extinction up to 20-fold larger than the physical cross sections of the particles. As the resonances become sharper, the peak intensity of the resonance increases [83]. Many organic fluorophores in current use have relatively narrow emission spectra and their emission is likely to be enhanced by such structures. Metallic structures of the type shown in Figures 22 and 23 may be used with Qdots and lanthanides, both of which have emission spectra more narrow than typical fluorophores.

Wavelength-selective enhancement may not be limited to the type of structure shown in Figures 22 and 23. Various nanofabrication methods have been used to produce a variety of metal shapes bound to substrates [84-86]. Figure 24 shows an electron micrograph of nanotriangles on a glass substrate [86]. These triangles are formed by nanosphere lithographs (NSL) in which a regular array of polymeric beads are coated with a metal film. When the polymeric beads are removed, the metal deposited between the beads remains on the substrate, typically with a triangular shape.

Metallic shapes prepared by NSL have been shown to display a variety of extinction spectra. Depending on particle size and shape the resonances can be wide or narrow, can be dominated by a single resonance, or show multiple resonances at different wavelengths. Even a relatively simple fabrication method like NSL can be used to prepare particles that display resonances over a wide range of wavelengths (Figure 25). Shaped particles on substrates could provide plasmonic structures that enhance emission over a small range of wavelengths. If the particle spacing is varied gradually or stepwise, different wavelengths may be enhanced at different locations in the device, thereby providing spectral information about the sample from the spatial distribution of the emission.

In addition to shapes, clusters of metal particles may be used for wavelength-selective enhancement. Figure 26 summarizes data obtained for clusters of one, two, or three particles [87]. The numbers of particles at each location can be seen in the electron micrograph (top left). When illuminated with white light, different colors of scattered light are seen for different clusters. Each type of clusters shows distinct scattering spectra. A single particle scatters light most effectively at 710 nm, a cluster of two particles scatters light at 480 nm, and a cluster of three particles scatters light at 470 and 690 nm. We expect such clusters to work in the reverse direction. That is, when in contact with a solution containing fluorophores emitting at different wavelengths, the emission of each fluorophore will be enhanced to a different extent by each type of particle cluster.

Particle clusters of the type shown in Figure 24 could also be useful in studies of energy transfer or for detection of a biomolecule of interest that is expected to contain two different bound fluorophores. Consider the flow cell shown in Figure 27. Each region of the flow chamber could contain particle clusters bound to the walls or suspended in a porous matrix. As the donor (D) and acceptor (A) labeled sample flowed past the particles the enhancement would occur first for D, then for A, and then for both D and A. It is logical to question how such a structure (Figure 27) could be constructed. At present, these structures are created using various

lithographic methods. However, it is now known that silver and gold can be deposited in metallic form by simple irradiation with light [88-91]. Silver metals can also be deposited using light by a multiphoton process [92], which suggests the creation of three-dimensional structure laser scanning optics.

In the preceding paragraphs we described wavelength-selective enhancements using particles fixed to a substrate. It may also be of interest to obtain wavelength-selective enhancements in solution. Such particles may be useful in multiplex assays. Assays of this type require an ability to create solid particles or shells with a narrow resonance at the desired wavelength. Fortunately, a variety of such particles has been made using batch chemistries suitable for preparation of reasonable quantities of particles [93-95]. Figure 28 shows calculated scattering spectra of silver or gold nanoshells on a silica core [96]. The peak scattering wavelength, and presumably the peak wavelength for fluorescence enhancement, can be varied throughout the visible and NIR wavelengths. Changes in the peak scattering wavelengths are obtained by variation of the size and thickness of the core and shell, while keeping the overall diameter constant. We note that the configurations shown in the preceding figures are only meant to show that a variety of geometries are possible for wavelength-selective enhancements. It is likely that the eventual devices will have very different geometries.

In suggesting structures for enhanced fluorescence, we make an assumption that the fluorescence enhancement was in some way proportional to the strength of the plasmon resonance and to the extent of spectral overlap between this resonance and the emission spectrum of the fluorophore. This assumption seems reasonable, but, until recently, the supporting data have been limited. However, this situation is changing rapidly as other laboratories are becoming engaged in fluorophore-metal interactions. Figure 29 shows the geometry of a structure containing Qdots [97]. The Qdots are in PMMA and the silver cylinders penetrate the polymer. The reflectance spectra and, hence, plasmon resonance of the structure depend on the size and spacing of the cylinders (Figure 30, top). The emission spectra of the Qdots (bottom) show the largest enhancements when the plasmon resonance overlaps the Qdot emission spectrum. The extent of the enhancement was as large as 50-fold. The brightness of the Qdots depended upon the entire silver structure, not only the cylindrical posts. The Qdot emission was much higher when the silver cylinders were in contact with a continuous silver surface (Figure 31). These results show that structures for enhanced fluorescence can be designed using the assumption that a strong plasmon resonance is needed for maximum enhancements. However, this need not always be the case if the plasmon extinction is due to absorption rather than scattering.

Plasmon engineering

The phenomenon of surface plasmon-coupled emission (SPCE) shows that excited-state fluorophores can undergo a near-field nonradiative interaction with the metal to create propagating far-field radiation. This statement is supported by the observation of SPCE using silver, gold, and aluminum, with wavelengths ranging from the UV for tryptophan through the visible and extending to NIR wavelengths [98-102]. SPCE has also been observed with Qdots [103]. These diverse results suggest that near-field coupling of excited-state fluorophores with continuous metal surfaces is a general phenomenon that can be reliably predicted and utilized.

Surface plasmons are two-dimensional waves with optical frequencies which are trapped at an interface. This is an unusual phenomenon because light usually propagates freely in three dimensions. We are all aware of the remarkably complex electronic circuits that can be created because electrical currents can be manipulated on a flat surface. In contrast, optical devices such as waveguides and optical filter waveguides have the dimensions of light in three dimensions, and there are strict rules of reflection and refraction to change the direction of the

propagation wave. The different ways we manipulate light and electrical current are ingrained in our thinking so that we rarely consider controlling light in the same way we control electrical currents.

Surface plasmons are, in a sense, light transformed into current. It is known that surface plasmons can migrate considerable distances in thin metal films with modest attenuation and that plasmons can propagate in subwavelength size metallic structures [104-107]. This confinement property of plasmons is of interest for the design of components for optical computing. The ability to control the flow of optical energy in two-dimensions would have a profound impact on the design of devices for fluorescence sensing. Instead of using optical components to manipulate light, the fluorescence could be trapped in metallic nanostructures in the form of plasmons and moved to a different location on the surface. This capability would be useful in lab-on-a-chip or DNA array applications, where the chemistry is already on a surface, which can easily be a metal surface.

What is the evidence that plasmons can migrate usefully long distances without being dissipated by heat or by radiation into the substrate? How can the migrating plasmons be controlled? A relatively recent experiment has shown that plasmons with frequencies for wavelengths of 633 to 785 nm can migrate 50 to 150 μm with 1/*e* attenuation [108]. The detector was shielded from the incident light by the 50-nm aluminum film (Figure 32). It was found that the plasmons migrated further than expected if one accounted for attenuation due to radiation into the substrate. This radiation may have been prevented by the aluminum. The important point is that using available thin-film technology, one can create structures that allow plasmons to propagate or to radiate, depending on the local metal structure.

The use of plasmonic circuits requires ways to create directional plasmons and to reflect, diffract, or focus the energy. These manipulations of plasmons are now becoming possible [109]. Figure 33 shows how directional surface plasmons can be created by laser illumination of a silver wire on a silver film. The plasmons are seen to be strongly directional and to migrate distances greater than 10 μm. The next step for plasmon circuits is the fabrication of optical elements on a metal surface to manipulate the plasmons. This can now be accomplished using dielectric or metallic features on a metal film [110-112]. Two examples are shown in Figure 34. The plasmons are launched by irradiation of linear feature seen as a vertical line, similar to Figure 33. The bottom panels in Figure 34 show a plasmon mirror created by five rows of dots. This mirror has a reflectivity of 90%. The top panels show a beam splitter, which divides the plasmons reflected from the mirror.

Another example of plasmon engineering is the use of two-dimensional lenses to focus the plasmons. In one such example, a plasmon lens was made from a semicircle of nanoholes in a metal film [113]. The intensities of the plasmon fields were measured using NSOM (Figure 35). The plasmons were found to form a focal point, which was explained by interference at the plasmon wavelength. The focal point could be formed or eliminated by rotation of the incident polarization. The results in Figures 32, 33, 34, and 35 show that optical frequency energy can be transported and manipulated in a two-dimensional surface.

So far we have shown that it is possible to couple the energy of excited fluorophores into plasmons (via SPCE), transport the plasmons across a surface, and to manipulate the direction of the plasmons (Figures 32-35). In order to detect the energy it may be necessary to convert the plasmons back into propagating light. This conversion can be accomplished with simple two-dimensional structures [110]. Figure 36 (top) shows an SEM image of two nanohole arrays in a smooth gold film separated by 30 μm. The smaller array on the right, which is difficult to see in the figure, is illuminated at 815 nm, creating plasmons that migrate to the left. The bottom panel shows a near-field optical image of the sample. The plasmons migrate from right to left

between the arrays, and are converted back to visible light when they encounter the nanohole array on the left. Hence, plasmons can be created in one region of a device, propagate a reasonable distance, and then be converted back into light.

The ability to interconvert light and plasmons and to manipulate the plasmons can result in a new generation of devices for diagnostics, biotechnology, and other applications. Using currently available knowledge about plasmonics and fluorescence, one can propose a variety of configurations. Using the information in this article, one can imagine the device in Figure 37. The sample could be in a nanohole array designed to couple in the incident light or couple to the emission frequency from surface-bound fluorophores. The excited-state energy could migrate as plasmons on the smooth silver surface. The desired wavelengths could be converted back to light using nanohole arrays with different spacing, gratings, or using clusters of nanodots. Such a device would be inexpensive and easy to manufacture with available lithographic methods.

Multiphoton excitation near metallic structures

Multiphoton excitation (MPE) has become widely used in cellular imaging [114]. This application is possible because of the availability of Ti:sapphire lasers with 100-fs pulse widths and because the cell samples on slides are not strongly scattering. The presence of scattering decreases the peak power of the laser pulse and hence the extent of MPE. Because of the need for high peak powers, and to minimize the overall exposure of the sample to irradiation, MPE microscopy is accomplished almost completely with laser scanning optics.

The plasmon resonance in metal particles provides an opportunity for localized MPE near the particle. It is known that the incident fields can be dramatically amplified near nonspherical particles [115,116]. Calculations for a silver ellipsoid shows an enhanced field near the tips (Figure 38). The peak enhancement for the ellipsoid is a factor of 4700, which is above the range of the color scale in this figure. For a triangle, the enhanced fields are also located near the tips, with a peak enhancement of 3500-fold. A 4000-fold increase in intensity would result in a 16×10^6-fold enhancement for two-photon excitation. One laboratory has already reported a 10^5-fold enhancement of two-photon incident fluorescence near silver particles [117].

Even more dramatic field enhancements are expected near clusters of particles [116]. For example, the field between two closely spaced silver particles can be enhanced by a factor of 10^4 (Figure 39). This result predicts that two-photon excitation between the particles would be increased by a factor of 10^8. At first glance, a factor of 10^8 seems too large to be reasonable. However, surface-enhanced Raman scattering (SERS) is known to occur near silver clusters, and the bulk enhancement can be large. Like two-photon excitation, SERS is also a two-photon process, so both phenomena are expected to show large enhancements. An appropriately designed metal structure can act like an antenna and show resonance enhancements of the fields between the particles [118], which suggest another approach for localized MPE.

Enhanced multiphoton excitation can have applications to molecular imaging. A particle can be targeted to bind to a cell membrane or receptor protein using antibodies. Because of the enhanced field near the particles, MPE may occur only near the particles, providing information about the nearby biomolecules. One report has already appeared showing localized excitation of autofluorescence occurring near gold particles in living cells [119].

Subwavelength microscopy

Optical microscopy is an important tool for cellular imaging. Optical imaging is accomplished using a variety of methods including wide-field imaging, multiphoton excitation. and/or laser scanning confocal microscopy. Based on the Rayleigh criteria, the spatial resolution is limited

to about $\lambda/2$. This resolution can be increased using complex methods such as 4Pi, stimulated emission depletion, or near-field scanning microscopy [120], but the complexity and limitations of these methods have prevented their widespread use for cellular imaging.

The use of plasmonics offers the opportunity for subwavelength resolution microscopy, with a spatial resolution as small as 25 nm. This possibility can be traced to the reports of anomalously high transmission of light through arrays of nanoholes in metals [121] and to the prediction of a perfect lens based on negative materials [122]. It is known that the transmission efficiency of light decreases dramatically as the size of the aperture becomes smaller than the wavelength. Unexpectedly high transmission efficiencies were observed for apparently opaque silver films that contained arrays of holes with sizes ranging from about 50 to 150 nm. This observation resulted in additional studies with metal films containing various types of periodic structures [123-126]. One interesting example is the beaming transmission of light through a subwavelength aperture surrounded by concentric rings in the metal film [127]. The 300-nm-thick silver film does not transmit light in the absence of an aperture and grooves. When the 250-nm aperture is surrounded by concentric rings, the transmitted light was found to beam with a sharp angular distribution (Figure 40). In the absence of concentric rings, the light was fully diffracted into half-space, as expected from classical optics (Figure 40).

The possibility of subwavelength resolution is of great interest for nanotechnology. It is now known that the near fields from surface plasmons can have dimensions much smaller than free-space radiation at the same frequency [128-132]. The size of the optical near fields was studied by illumination of a photoresist through a nanohole array as shown in Figure 41. Exposure to the photoresist through this nanohole array resulted in features spaced by 170 nm with a feature size of 90 nm [131]. This result demonstrates that the electric fields near the metal films have dimensions near 90 nm (Figure 42). By the use of slightly more complex structures, the near fields can have dimensions of 25 nm [129,132].

The concepts of plasmon-coupled transmission and optical near fields are merging into proposals for wide-field optical microscopy with subwavelength resolution [133-135]. Such a microscope could be based on excitation of the specimen by the near field near the nanohole array. It is now thought that the near fields are tightly confined, or at least not diffracted into half-space, as will occur without plasmon-coupled transport (Figure 43). In order to construct a microscope, it would be necessary to measure the intensities from fluorophores excited by the near fields with subwavelength dimensions. The emission from these regions could be imaged if the nanoholes were about 1 μm apart (Figure 44). The fluorescence excited near each nanohole could be imaged onto an array detector. The specimen or nanohole array would be moved and the multiple images used to reconstruct the entire image.

Construction of such a microscope faces several technological challenges, such as positioning and moving the specimen and array relative to each other, and obtaining near fields with subwavelength dimensions at reasonable distances from the metal. The extensive interest in nanolithography is already resulting in methods to control and focus the near fields. In a limited sense, this approach to subwavelength imaging is already in use [136,137]. Figure 45 shows an experimental arrangement that provides for excitation of a subwavelength region of a cell membrane. The cell is positioned near a single nanohole in an aluminum film. Electrodynamics calculations for this system indicate that the light does not penetrate into the nanohole but does create a field in the hole on the surface of incidence. Fluorescence correlation spectroscopy (FCS) measurements indicated that only a 100-nm region of the membrane was excited. Of course, this approach would not allow whole-cell imaging because of the need to move the illuminated spots. Although there are certain to be many technical challenges, we are not aware of any physical limits that would prevent creation of a subwavelength plasmonic microscope.

Conclusion

The combination of fluorescence with plasmonics will result in a paradigm shift for both technologies. Fluorescence instrumentation, devices, and sensors will begin to use plasmons for creation of excited states and manipulation of the emission energy. The field of plasmonics will expand to include studies of the factors that govern fluorophore-metal interactions and of how to optimize the desired effects. These new approaches to fluorescence and plasmonics will be facilitated by the rapid growth of nanofabrication methods, resulting in new approaches to high-through-put biology, diagnostics, and molecular imaging.

Acknowledgments

This study was supported by the NIH National Center for Research Resources (RR08119), NHGRI HG-002655 and NIBIB EB000682.

References

1. Lakowicz JR. Radiative decay engineering: biophysical and biomedical applications. Anal Biochem 2001;298:1–24. [PubMed: 11673890]
2. Lakowicz JR, Shen Y, D'Auria S, Malicka J, Fang J, Gryczynski Z, Gryczynski I. Radiative decay engineering 2. Effects of silver island films on fluorescence intensity, lifetimes, and resonance energy transfer. Anal Biochem 2002;301:261–277. [PubMed: 11814297]
3. Chance RR, Prock A, Silbey R. Molecular fluorescence and energy transfer near interfaces. Adv Chem Phys 1973;37:1–65.
4. Ford GW, Weber WH. Electromagnetic interactions of molecules with metal surfaces. Phys Rep 1984;113(4):195–287.
5. Gersten J, Nitzan A. Spectroscopic properties of molecules interacting with small dielectric particles. J Chem Phys 1981;75(3):1139–1152.
6. Gersten, JI. Theory of fluorophore-metallic surface interactions. In: Geddes, CD.; Lakowicz, JR., editors. Topics in Fluorescence Spectroscopy vol 8: Radiative Decay Engineering. Springer Science +Business Media, Inc; New York: 2005. p. 197-221.
7. Geddes, CD.; Aslan, K.; Gryczynski, I.; Malicka, J.; Lakowicz, JR. Radiative decay engineering. In: Geddes, CD.; Lakowicz, JR., editors. Topics in Fluorescent Spectroscopy vol 8: Radiative Decay Engineering. Springer Science+Business Media, Inc; New York: 2005. p. 405-448.
8. Geddes, CD.; Aslan, K.; Gryczynski, I.; Malicka, J.; Lakowicz, JR. Noblemetal surfaces for metal enhanced fluorescence. In: Geddes, CD.; Lakowicz, JR., editors. Topics in Fluorescent Spectroscopy, vol 8: Radiative Decay Engineering. Springer Science+Business Media, Inc; New York: 2005. p. 365-401.
9. Lakowicz JR. Radiative decay engineering 3. Surface plasmon-coupled directional emission. Anal Biochem 2004;324:153–169. [PubMed: 14690679]
10. Gryczynski I, Malicka J, Gryczynski Z, Lakowicz JR. Radiative decay engineering 4. Experimental studies of surface plasmon coupled directional emission. Anal Bio-chem 2004;324:182–270.
11. Benner RE, Dornhaus R, Chang RK. Angular emission profiles of dye molecules excited by surface plasmon waves at a metal surface. Opt Commun 1979;30(2):145–149.
12. Pockhand I, Brilliante A, Mobius D. Nonradiative decay of molecular excitation at a metal interface. Nuovo Cim 1980;63:350–357.
13. Hayashi S. Spectroscopy of gap modes in metal particle-surface systems. Top Appl Phys 2001;81:71–95.
14. Gerbshtein YM, Merkulov IA, Mirlin DN. Transfer of luminescence-center energy to surface plasmons. JETP Lett 1975;22:35–36.
15. Zhang J, Gryczynski Z, Lakowicz JR. First observation of surface plasmon-coupled electrochemiluminescence. Chem Phys Lett 2004;393:483–487. [PubMed: 19763232]
16. Lakowicz JR. Radiative decay engineering 5: metal-enhanced fluorescence and plasmon emission. Anal Bio-chem 2005;337:171–194.

17. Bohren, CF.; Huffman, DR. Absorption and Scattering of Light by Small Particles. John Wiley & Sons, Inc; New York: 1983. p. 530
18. Kreibig, U.; Vollmer, M. Optical properties of metal clusters. In: Gonser, U.; Osgood, RM.; Panish, MB.; Sakaki, H., editors. Materials Science. Springer; New York: 1995. p. 532
19. Born, M.; Wolf, E. Principles of Optics. Vol. 7th ed.. Cambridge University Press; 2002. Electromagnetic theory of propagation, interference and diffraction of light; p. 952
20. Griffiths, DJ. Introduction to Electrodynamics. Prentice Hall; New Jersey: 1999. p. 516
21. Aslan K, Leonenko Z, Lakowicz JR, Geddes CD. Fast and slow deposition of silver nanorods on planar surfaces: application to metal-enhanced fluorescence. J Phys Chem B 2005;109:3157–3162. [PubMed: 16851335]
22. Zhang J, Lakowicz JR. Enhanced luminescence of Phenyl-phenenthridine dye on aggregated small silver nanoparticles. J Phys Chem B 2005;109:8701–8706. [PubMed: 16852030]
23. Zhang J, Malicka J, Gryczynski I, Lakowicz JR. Surface enhanced fluorescence of fluorescein-labeled oligonucleotides capped on silver nanoparticles. J Phys Chem B 2005;109:7643–7648. [PubMed: 16851886]
24. Zhang J, Malicka J, Gryczynski I, Lakowicz JR. Oligonucleotide-displaced organic monolayer-protected silver nanoparticles and enhanced luminescence of their salted aggregates. Anal Biochem 2004;330:81–86. [PubMed: 15183765]
25. Tominaga, J. The manipulation of surface and local plasmons. In: Tsai, DP., editor. Optical Nanotechnologies. Springer; New York: 2003. p. 212
26. Ohtsu, M.; Kobayashi, K. Optical Near Fields. Springer; New York: 2004. Introduction to classical and quantum theories of electromagnetic phenomena at the nanoscale; p. 205
27. Kawata, S.; Ohtsu, M.; Irie, M., editors. Nano-Optics. Springer; New York: 2002. p. 321
28. Wood RH. Anomalous diffraction gratings. Phys Rev 1935;48:928–937.
29. Hutley MC, Maystre D. The total absorption of light by a diffraction grating. Opt Commun 1976;19 (3):431–436.
30. Ebbesen TW, Lezec HJ, Ghaemi HF, Thio T, Wolf PA. Extraordinary optical transmission through subwavelength hole arrays. Lett Nat 1998;390:667–669.
31. Lezec HJ, Degiron A, Devaux E, Linke RA, Martin-Moreno L, Garcia-Vidal FJ, Ebbesen TW. Beaming light from a subwavelength aperture. Science 2002;297:820–822. [PubMed: 12077423]
32. Sullivan, DM. Electromagnetic simulation using the FDTD method. In: Pollard, RD.; Booton, R., editors. IEEE Microwave Theory and Techniques. The Institute of Electrical and Electronics Engineers, Inc; New York: 2000. p. 165
33. Taflove, A.; Hagnes, SC. Computational Electrodynamics: The Finite Difference Time-Domain Method. Vol. 2nd ed.. Artech House; Boston and London: 2000. p. 852
34. Hanken DG, Jordan CE, Frey BL, Corn RM. Surface plasmon resonance measurements of ultrathin organic films at electrode surfaces. Electroanal Chem 1998;20:141–225.
35. Ivarsson, B.; Malmqvist, M. Development and use of BIACORE instruments for biomolecular interaction analysis. In: Gizeli, E.; Lowe, CR., editors. Biomolecular Sensors. Taylor and Francis; London: 2002. p. 322
36. Raether, H. Surface Plasmons on Smooth and Rough Surfaces and on Gratings. Springer-Verlag; New York: 1988. p. 136
37. Raether, H. Surface plasma oscillations and their applications. In: Hass, G.; Francombe, MH.; Hoffman, RW., editors. Physics of Thin Films. Academic Press; New York: 1978. p. 145-261.
38. Forstmann F, Gerhardts RR. Metal optics near the plasma frequency. Springer Tracts Mod Phys 1986;109:132.
39. Kelly KL, Coronado E, Zhao LL, Schatz GC. The optical properties of metal nanoparticles: the influence of size, shape, and dielectric environment. J Phys Chem B 2003;107:668–677.
40. Bohren, CF.; Huffman, DR. Absorption and Scattering of Light by Small Particles. John Wiley and Sons, Inc; New York: 1983. p. 530
41. Yguerabide J, Yguerabide EE. Light scattering submicroscopic particles as highly fluorescent analogs and their use as tracer labels in clinical and biological applications. Anal Biochem 1998;262:137–156. [PubMed: 9750128]

42. Schultz DA. Plasmon resonant particles for biological detection. Curr Opin Biotechnol 2003;14:13–22. [PubMed: 12565997]
43. Cao YW, Jin R, Mirkin CA. DNA-modified core-shell Ag/Au nanoparticles. J Am Chem Soc 2001;123:7961–7962. [PubMed: 11493092]
44. Jin R, Wu G, Li Z, Mirkin CA, Schatz GC. What controls the melting properties of DNA-linked gold nano-particle assemblies? J Am Chem Soc 2003;125:1643–1654. [PubMed: 12568626]
45. Enderlein, J.; Zander, C. Theoretical foundations of single molecule detection in solutions. In: Zander, Ch; Endelein, J.; Keller, RA., editors. Single Molecule Detection in Solution. Wiley-VCH; Germany: 2002. p. 371
46. Schultz S, Smith SR, Mock JJ, Schulz DA. Single target molecule detection with nonbleaching multicolor optical immunolabels. Proc Natl Acad Sci USA 2000;97:996–1001. [PubMed: 10655473]
47. Kyriacou SV, Brownlow WJ, Xu XH. Using nanoparticle optics assay for direct observation of the function of antimicrobial agents in single live bacterial cells. Biochemistry 2004;43:140–147. [PubMed: 14705939]
48. Sokolov K, Follen M, Aaron J, Pavlova I, Malpica A, Lotan R, Richards-Kortum R. Real-time vital optical imaging of precancer using anti-epidermal growth caftor receptor antibodies conjugated to gold nanoparticles. Cancer Res 2003;63:199–2004.
49. Mitchell JS, Wu Y, Cook CJ, Main L. Sensitivity enhancement of surface plasmon resonance biosensing of small molecules. Anal Biochem 2005;343:125–135. [PubMed: 15950915]
50. He L, Smith EA, Natan MJ, Keating DD. The distance dependence of colloidal Au-amplified surface plasmon resonance. J Phys Chem B 2004;108:10973–10980.
51. He L, Musick MD, Nicewarner SR, Salinas FG, Benkovic SJ, Natan MJ, Keating CD. Colloidal Au-enhanced surface plasmon resonance for ultrasensitive detection of DNA hybridization. J Am Chem Soc 2000;122:9071–9077.
52. Enderlein J. Spectral properties of a fluorescing molecule within a spherical metallic cavity. Phys Chem Chem Phys 2002;4:2780–2786.
53. Enderlein J. Theoretical study of single molecule flouresence in a metalic nanocavity. Appl Phys Lett 2002;80:315–317.
54. Lakowicz JR, Malicka J, D'Auria S, Gryczynski I. Release of the self-quenching of fluorescence near silver metallic surfaces. Anal Biochem 2003;320:13–20. [PubMed: 12895465]
55. Scheim S, Smith GB. Internal electrical field densities of metal nanoshells. J Phys Chem B 2005;109:1689–1694. [PubMed: 16851144]
56. Jaiswal JK, Mattoussi H, Mauro JM, Simon SM. Long-term multiple color imaging of live cells using quantum dot bioconjugates. Nat Biotechnol 2003;21:47–51. [PubMed: 12459736]
57. Osaki F, Kanamori H, Sando S, Sera T, Aoyama Y. A quantum dot conjugated sugar ball and its cellular uptake. On the side effects of endocytosis in the subviral region. J Am Chem Soc 2004;126:6520–6521. [PubMed: 15161257]
58. Smith AM, Gao X, Nie S. Quantum dot nanocrystals for *in vivo* molecular and cellular imaging. Photochem Photobiol 2004;80:377–385. [PubMed: 15623319]
59. Michalet X, Pinaud FF, Bentolila LA, Tsay JM, Doose S, Li JJ, Sundaresan G, Wu AM, Gambhir SS, Weiss S. Quantum dots for live cells *in vivo* imaging and diagnostics. Science 2005;307:538–544. [PubMed: 15681376]
60. Jiang W, Papa E, Fischer H, Mardyani S, Chan WC. Semiconductor quantum dots as contrast agents for whole animal imaging. Trends Biotech 2004;22(12):604–609.
61. Derfus AM, Chan WC, Bhatia SN. Probing the cytotoxicity of semiconductor quantum dots. Nano Lett 2004;4(1):11–18.
62. Murphy CJ, Coffer JL. Quantum dots: a primer. Appl Spectrosc 2002;56:16A–27A.
63. Rosenthal SJ. Barcoding biomolecules with fluorescent nanocrystals. Nat Biotechnol 2001;19:621–622. [PubMed: 11433268]
64. Wang H, Goodrich GP, Tam F, Oubre C, Nordlander P, Halas NJ. Controlled texturing modifies the surface topography and plasmonic properties of Au nanoshells. J Phys Chem B 2005;109:11083–11087. [PubMed: 16852350]

65. Shi W, Sahoo Y, Swihart MT, Prasad PN. Gold nanoshells on polystyrene cores for control of surface plasmon resonance. Langmuir 2005;21:1610–1617. [PubMed: 15697315]

66. Pawley, JB., editor. Handbook of Biological Confocal Microscopy. Vol. 2nd ed.. Plenum Press; New York: 1995. p. 632

67. Xu, C.; Webb, WW. Multiphoton excitation of molecular fluorophores and nonlinear laser microscopy. In: Lakowicz, JR., editor. Topics in Fluorescence Spectroscop, vol 5: Nonlinear and Two-Photon Induced Fluorescence. Plenum Press; New York: 1997. p. 471-545.

68. Wallrabe H, Periasamy A. Imaging protein molecules using FRET and FLIM microscopy. Curr Opin Biotechnol 2005;16(1):19–27. [PubMed: 15722011]

69. Clegg, RM. Fluorescence resonance energy transfer. In: Wang, XF.; Herman, B., editors. Fluorescence Imaging Spectroscopy and Microscopy. John Wiley & Sons; New York: 1996. p. 473

70. Nelson, DL.; Cox, MM. Lehninger Principles of Biochemistry. Vol. 4th ed.. WH Freeman and Co; New York: 2005.

71. Su K-H, Wei Q-H, Zhang X, Mock JJ, Smith DR, Schultz S. Interparticle coupling effects on plasmon resonances of nanogold particles. Nano Lett 2003;3(8):1087–1090.

72. Gunnarsson L, Rindzevicius T, Prikulis J, Kasemo B, Käll M, Zou S, Schatz GC. Confined plasmons in nanofabricated single silver particle pairs: experimental observations of strong interparticle interactions. J Phys Chem B 2005;109:1079–1087. [PubMed: 16851063]

73. Sokolov K, Follen M, Aaron J, Pavlova I, Malpica A, Lotan R, Richards-Kortum R. Real-time vital optical imaging of precancer using anti-epidermal growth factor receptor antibodies conjugated to gold nanoparticles. Cancer Res 2003;63:199–2004.

74. Sonnichsen C, Reinhard BM, Liphardt J, Alivistos AP. A molecular ruler based on plasmon coupling of single gold and silver nanoparticles. Nat Biotechnol 2005;23(6):741–745. [PubMed: 15908940]

75. Nordlander P, Prodan E. Plasmon hybridization in nanoparticles near metallic surfaces. Nano Lett 2004;4(11):2209–2213.

76. Rechberger W, Hohenau A, Leitner A, Krenn JR, Lamprecht B, Aussenegg FR. Optical properties of two interacting gold nanoparticles. Opt Commun 2003;220:137–141.

77. Brioude A, Jiang XC, Pileni MP. Optical properties of gold nanorods: DDA simulations supported by experiments. J Phys Chem B 2005;109:13138–13142. [PubMed: 16852635]

78. Park SY, Stroud D. Surface-plasmon dispersion relations in chains of metallic nanoparticles: an exact quasistatic calculation. Phys Rev B 2004;69:125418-1–125418-7.

79. Girard C, Quidant R. Near-field optical transmittance of metal particle chain wavelengths. Opt Express 2004;12:6141–6146. [PubMed: 19488257]

80. Panoiu NC, Osgood RM. Subwavelength nonlinear plasmonic nanowire. Nano Lett 2004;4:2427–2430.

81. Hicks EM, Zou S, Schatz GC, Spears KG, van Duyne R, Gunnarson L, Rindzevicius T, Kasemo B, Kall M. Controlling plasmon lineshapes through diffractive coupling linear arrays of cylindrical nanoparticles fabricated by electron beam lithography. Nano Lett 2005;5:1065–1070. [PubMed: 15943444]

82. Zou S, Janel N, Schatz GC. Silver nanoparticle array structures that produce remarkably narrow plasmon lineshapes. J Chem Phys 2004;120:10871–10875. [PubMed: 15268116]

83. Mulvaney P. Surface plasmon spectroscopy of nanosized metal particles. Langmuir 1996;12:788–800.

84. Zhang H, Mirkin CA. DPN-Generated nanostructures made of gold, silver, and palladium. Chem Mater 2004;16:1480–1484.

85. Childs WR, Nuzzo RG. Large area patterning of coinage-metal thin films using decal transfer lithography. Langmuir 2005;21:195–202. [PubMed: 15620303]

86. Haynes CL, Van Duyne RP. Nanosphere lithography: a versatile nanofabrication tool for studies of size-dependent nanoparticle optics. J Phys Chem B 2001;105:5599–5611.

87. Krenn JR, Aussenegg. Nanoptik mit metallischen Stukturen. Phys-J 2002;1:39–45.

88. Geddes CD, Parfenov A, Lakowicz JR. Photo-deposition of silver can result in metal-enhanced fluorescence. Appl Spectrosc 2003;57(5):526–531. [PubMed: 14658678]

89. Geddes CD, Parfenov A, Roll D, Fang J, Lakowicz JR. Electrochemical and laser deposition of silver for use in metal-enhanced fluorescence. Langmuir 2003;19(15):6236–6241.

90. Gutta P, Hoffmann R. Propensity of different AgBr surfaces for photo-induced silver cluster formation: a molecular orbital analysis. J Phys Chem A 2003;107:8184–8190.

91. Yamamoto T, Machi K, Nagare S, Hmamda K, Senna M. The relation between surface plasmon resonance and morphology of Ag nanorods prepared by pulse laser deposition. Solid State Ion 2004;172:299–302.

92. Bsldacchini T, Pons AC, Lafratta CN, Fourkas JT. Multiphoton laser direct writing of two-dimensional silver structures. Opt Express 2005;13:1275–1280. [PubMed: 19495000]

93. Liang HP, Wan LJ, Bai CL, Jiang L. Gold hollow nanospheres: tunable surface plasmon resonance controlled by interior cavity sizes. J Chem Phys B 2005;109:7795–7800.

94. Chen MMY, Katz A. Synthesis and characterization of gold-silica nanoparticles incorporating a mercaptosilane core-shell interface. Langmuir 2002;18:8566–8572.

95. Oldenburgh SJ, Westscott SL, Averitt RD, Halas NJ. Surface enhanced Raman scattering in the near infrared using metal nanoshell substrates. J Chem Phys 1999;111(10):4729–4735.

96. Chen K, Lui Y, Ameer G, Backman V. Optimal design if structured nanospheres for ultrashape light-scattering resonances as molecular imaging mutilabels. J Biomed Opt 2005;10(2):024005–024110. [PubMed: 15910079]

97. Song JH, Atay T, Shi S, Urabe H, Nurmiko AV. Large enhancement of fluorescence efficiency from CdSe/Zns quantum dots induced by resonant coupling to spatially controlled surface plasmons. Nano Lett 2005;5(8):1557–1561. [PubMed: 16089488]

98. Grycynski I, Mailicka J, Lukomska J, Grycynski Z, Lakowicz JR. Surface plasmon-coupled polarized emission of N-acetyl-l-tryptophanamide. Photochem, Photobiol 2004;80:482–485. [PubMed: 15623334]

99. Malicka J, Gryczynski I, Gryczynski Z, Lakowicz JR. Surface plasmon-coupled emission of 2,5-diphenyl-1,3,4-oxadiazole. J Phys Chem B 2004;108:19114–19118.

100. Gryczynski I, Malicka J, Gryczynski Z, Lakowicz JR. Surface plasmon-coupled emission with gold films. J Phys Chem B 2004;108:12568–12574.

101. Grycynski I, Malicka J, Grycynski Z, Nowaczyk K, Lakowicz JR. Ultraviolet surface-plasmon-coupled emission using thin aluminum films. Anal Chem 2004;76:4076–4081. [PubMed: 15253645]

102. Geddes CD, Grycynski I, Malicka J, Grycynski Z, Lakowicz JR. Directional surface plasmon coupled emission. J Fluoresc 2004;14(1):119–123. [PubMed: 15622871]

103. Gryczynski I, Malicka J, Jiang W, Fischer H, Chan W, Grycynski Z, Grudzinski W, Lakowicz JR. Surface-plasmon-coupled emission of quantum dots. J Phys Chem B 2005;109:1088–1093. [PubMed: 16851064]

104. Barnes WL, Dereux A, Ebbesen TW. Surface plasmon subwavelength optics. Nature 2003;424:824–830. [PubMed: 12917696]

105. Gramotnev DK, Pile DFP. Single-mode subwavelength waveguide with channel plasmon-polaritons in triangular grooves on a metal surface. Appl Phys Lett 2004;85:6323–6325.

106. Maier SA, Kik PG, Atwater HA, Meltzer S, Harrel E, Koel BE, Requicha AG. Local detection of electromagnetic energy transport below the diffraction limit in metal nanoparticle plasmon waveguides. Nat Mater 2003;2:228–232.

107. Brongersma ML, Hartman JW, Atwater HA. Electromagnetic energy transfer and switching in nanoparticle chain arrays below the diffraction limit. Phys Rev B 2000;62:356–359.

108. Lamprecht B, Krenn JR, Schider G, Ditlbacher H, Felidj N, Leitner A, Aussenberg FR. Surface plasmon propagation in microscale metal stripes. Appl Phys Lett 2001;79:51–53.

109. Ditlbacher H, Krenn JR, Felidj N, Lamprecht B, Schider G, Salerno M, Leitner A, Aussenberg FR. Fluorescence imaging of surface plasmon fields. Appl Phys Lett 2002;80:404–406.

110. Devaux E, Ebbesen TW, Weeber JC, Dereux A. Launching and decoupling surface plasmons via micrograting. Appl Phys Lett 2003;83:4936–4938.

111. Krenn JR, Ditlbacher H, Schider G, Hohenau A, Leitner A, Aussenberg FR. Surface plasmon micro- and nano optics. J Microsc 2003;209:167–172. [PubMed: 12641756]

112. Hohenau A, Krenn JR, Stepanov AL, Drezert A, Ditlbacher H, Steinberger B, Leitner A, Aussenberg FR. Dielectric optical elements for surface plasmons. Opt Lett 2005;30:893–895. [PubMed: 15865390]
113. Yin L, Vlasko-Vlasov VK, Pearson J, Hiller JM, Hua J, Welp U, Brown DE, Kimball CW. Subwavelength focusing and guiding of surface plasmons. Nano Lett 2005;5(7):1399–1402. [PubMed: 16178246]
114. Xu, C.; Webb, WW. Multiphoton excitation of molecular fluorophores and nonlinear laser microscopy. In: Lakowicz, JR., editor. Topics in Fluorescence Spectroscopy: Volume 5: Nonlinear and Two-Photon-Induced Fluorescence. Plenum Press; New York: 1997. p. 471-540.
115. Calander N, Willander M. Theory of surface-plasmon resonance optical field enhancement at prolate spheroids. J Appl Phys 2002;92:4878–4884.
116. Hao E, Schatz GC. Electromagnetic fields around silver nanoparticles and dimers. J Chem Phys 2004;120:357–366. [PubMed: 15267296]
117. Wenseleers W, Stellacio F, Meyer-Frederickson T, Mangel T, Bauer C, Pond SJK, Marder SR, Perry JW. Five orders-of-magnitude enhancement of two-photon absorption for dyes on silver nanoparticle fractal clusters. J Phys Cherm B 2002;106:6853–6863.
118. Muhlschlegel P, Eisler HJ, Martin OJF, Hecht B, Pohl DW. Resonant optical antennas. Science 2005;308:1607–1609. [PubMed: 15947182]
119. Yelin D, Oron D, Thiberge S, Moses E, Silberberg Y. Multiphoton plasmon-resonance microscopy. Opt Express 2003;11:1385–1391. [PubMed: 19466009]
120. Garini Y, Vermolen BJ, Young IT. From micro to nano: recent advances in high resolution microscopy. Curr Opin Biotechnol 2005;16:3–12. [PubMed: 15722009]
121. Ebbesen TW, Lezec HJ, Ghaemi HF, Thio T, Wolff PA. Extraordinary optical transmission through subwavelength hole arrays. Nature 1998;39:667–669.
122. Pendry JP. Negative refraction makes a perfect lens. Phys Rev Lett 2000;85:3966–3969. [PubMed: 11041972]
123. Thomas DA, Hughes HP. Enhanced optical transmission through a subwavelength 1D aperture. Solid State Commun 2004;129:519–524.
124. Martin-Moreno L, Garcia-Vidal FJ, Lezec HJ, Degiron A, Ebbesen TW. Theory of highly directional emission from a single subwavelength aperture surrounded by surface corrugations. Phys Rev Lett 2003;90:167401–167404. [PubMed: 12732005]
125. Luo X, Shi J, Wang H, Yu G. Surface plasmon polariton radiation from metallic photogenic crystal slabs breaking the diffraction limit: nano-storage and nanofabrication. Mod Phys Lett B 2004;18:945–953.
126. Sun Z, Kim HK. Refractive transmission of light and beam shaping with metallic nano-optic lenses. Appl Phys Lett 2004;85:642–644.
127. Lezec HJ, Degiron A, Devaux E, Linke RA, Martin-Moreno L, Garcia-Vidal FJ, Ebbesen TW. Beaming light from a subwavelength aperture. Science 2002;297:820–822. [PubMed: 12077423]
128. Hohng SC, Yoon YC, Kim DS, Malyachuk V, Muller R, Lienau Ch, Park JW, Yoo KH, Kim J, Ryu HY, Park QH. Light emission from the shadows: surface plasmon nano-optics at near light and far fields. Appl Phys Lett 2002;81:3239–3241.
129. Luo X, Ishihara T. Surface plasmon resonant interference nanolithography technique. Appl Phys Lett 2004;84:4780–4782.
130. Dragnea B, Szarko JM, Kowarik S, Weimann T, Feldmann J, Leone SR. Near-field surface plasmon excitation on structured gold films. Nano Lett 2003;3(1):3–7.
131. Srituravanich W, Fang N, Sun C, Luo Q, Zhang X. Plasmonic nanolithography. Nano Lett 2004;4 (6):1085–1088.
132. Liu Z-W, Wei Q-H, Zhang X. Surface plasmon interference nanolithography. Nano Lett 2005;5(5): 957–961. [PubMed: 15884902]
133. Smolyaninov II, Elliott J, Zayats AV, Davis CC. Farfield optical microscopy with a nanometer-scale resolution based on the in-plane image magnification by surface plasmon polaritons. Phys Rev Lett 2005;94:057401–057401-4. [PubMed: 15783692]

134. Garini Y, Kutchoukov VG, Bossche A, Alkemade PFA, Docter M, Verbeek PW, van Vliet LJ, Young IT. Toward the development of a three-dimensional mid-field microscope. Proc SPIE 2004;5327:115–122.

135. Docter MW, Young IT, Kutchoukov VG, Bossche A, Alkemade PFA, Garini Y. A novel concept for a mid-field microscope. Proc SPIE 2005;5703:118–126.

136. Levene MJ, Korlach J, Turner SW, Foquet M, Craighead HG, Webb WW. Zero-mode waveguides for single-molecule analysis at high concentrations. Science 2003;299:682–686. [PubMed: 12560545]

137. Edel JB, Wu M, Baird B, Craighead HG. High spatial resolution observation of single-molecule dynamics in living cell membranes. Biophys J 2002:L43–Ll45.

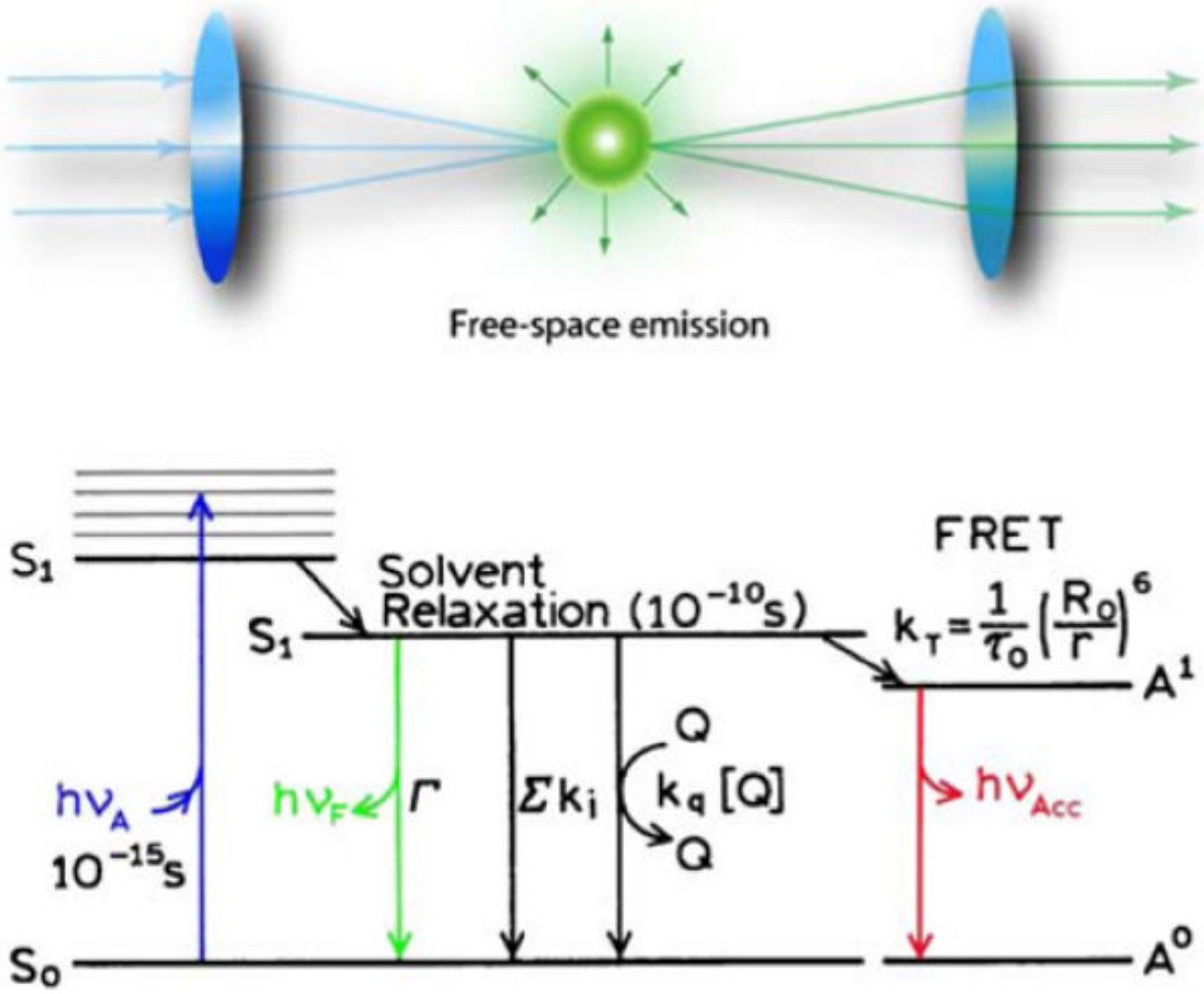

Figure 1.
Free-space emission.

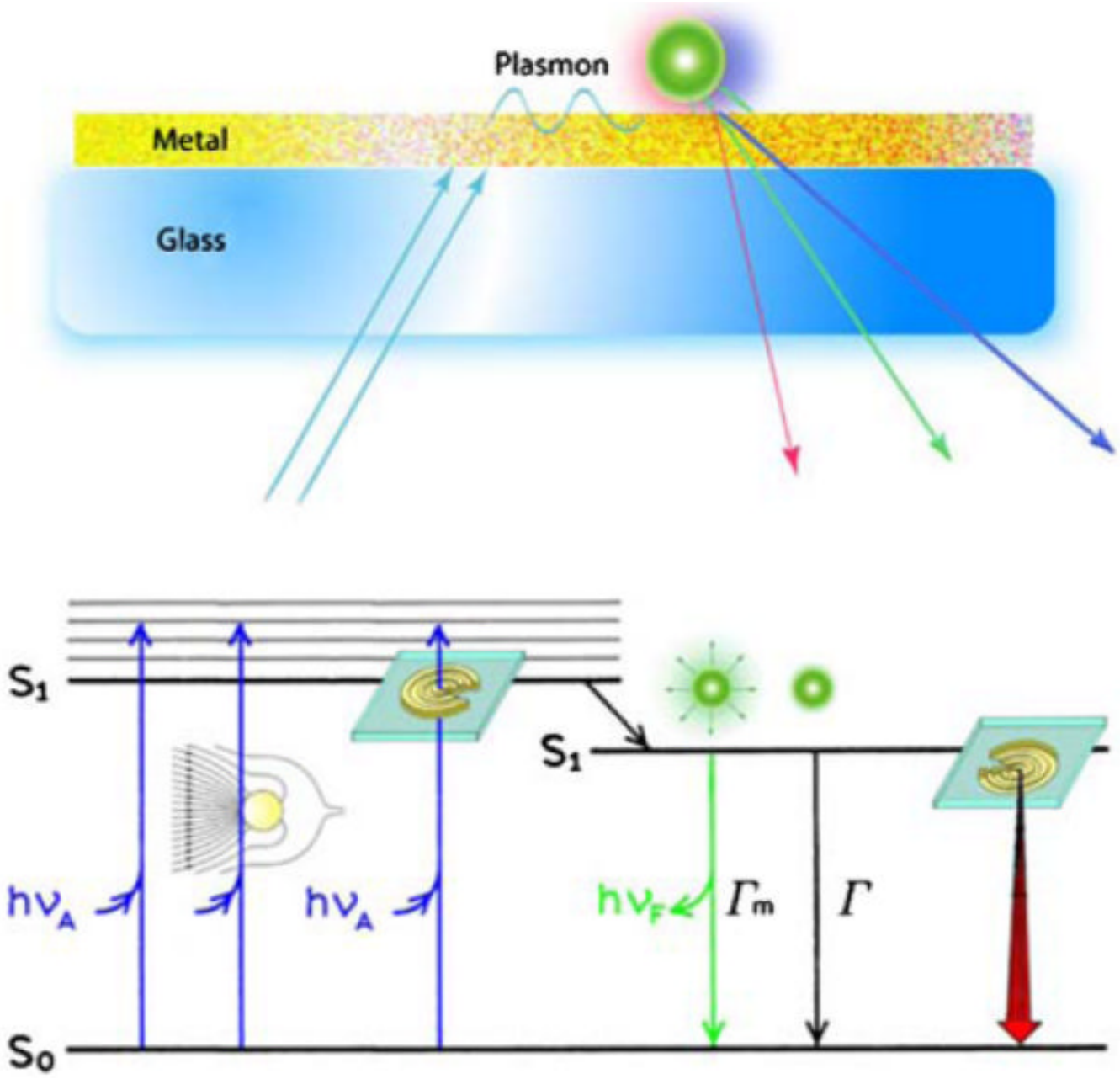

Figure 2.
Plasmon controlled emission.

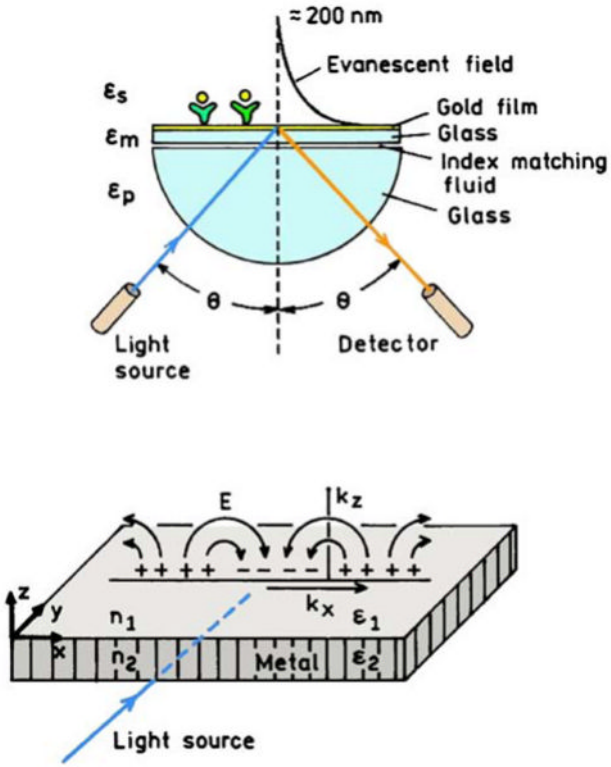

Figure 3.
Schematics of an SPR experiment (top) and of the light-induced surface plasmons (bottom).

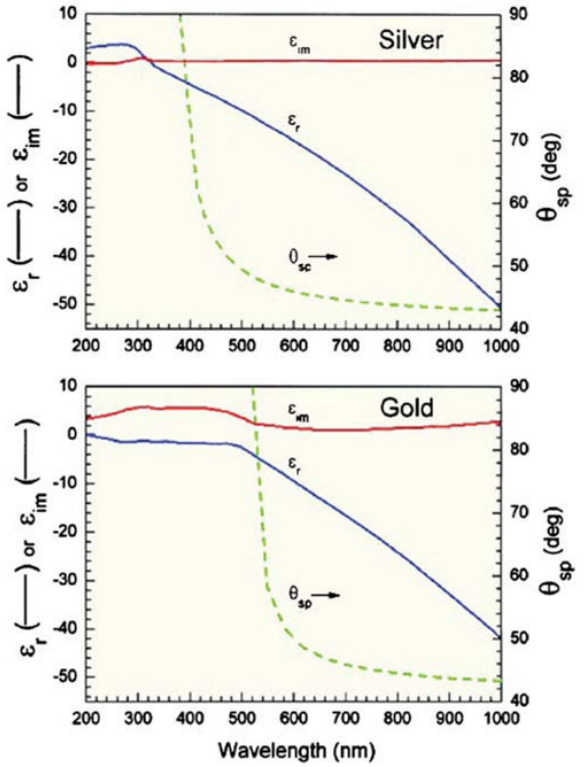

Figure 4.
Dielectric constants for silver and gold.

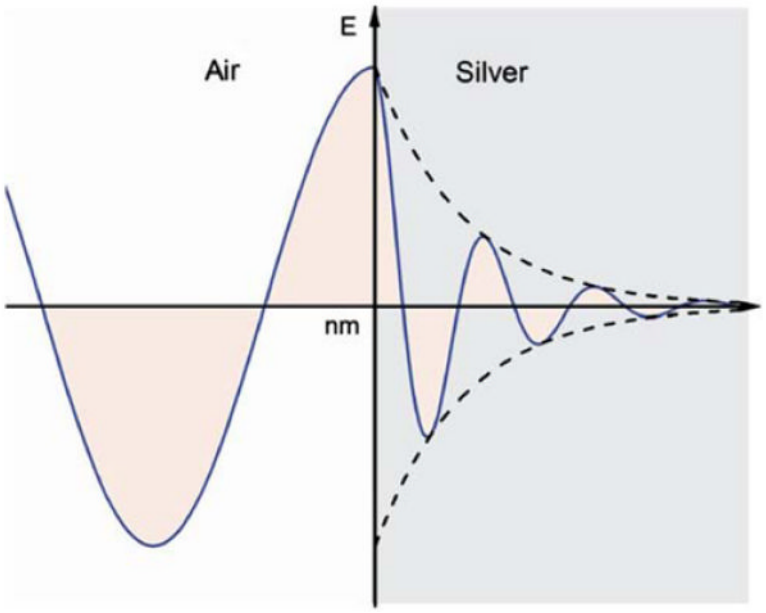

Figure 5.
Schematic of attenuation of 600 nm light on a metal surface.

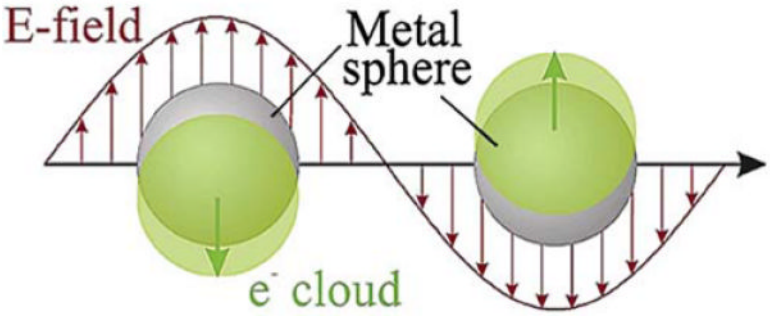

Figure 6.
Schematic of plasmon oscillation for a sphere. From [39].

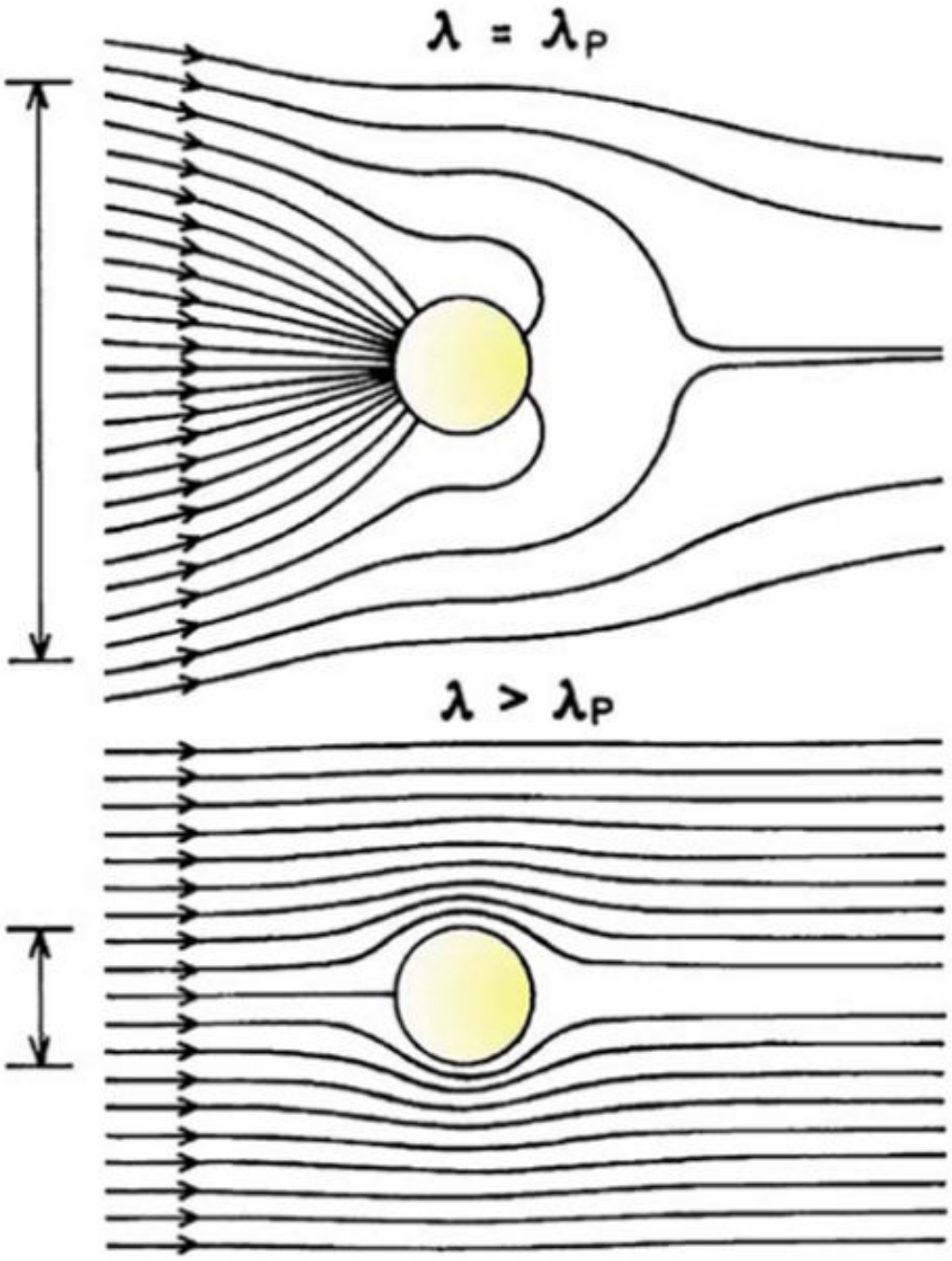

Figure 7.
Poynting vector or energy flow (lines) around a subwavelength metallic colloid illuminated at the plasmon wavelength (top) and at a wavelength longer than the plasmon wavelength (bottom). The vertical lines on the left indicate the diameter of the cross sections for absorption. This diagram does not show the energy flow due to scattered light. From [40].

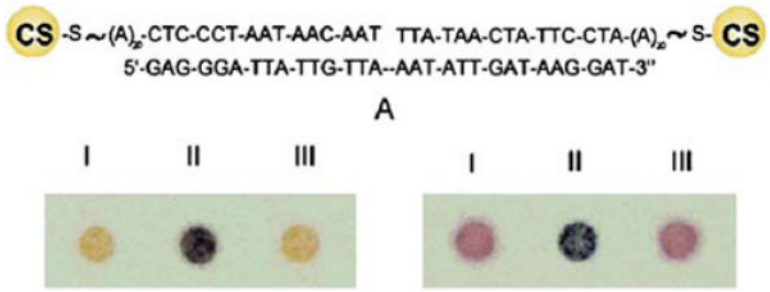

Figure 8.

Top, structure of metal particle-labeled DNA with a complementary oligomer. Bottom, photographs of the labeled DNA without target (I), with target (II), and with target at $T > T_m$. On the left are Ag/Au core shell particles. On the right are Au particles. From [43].

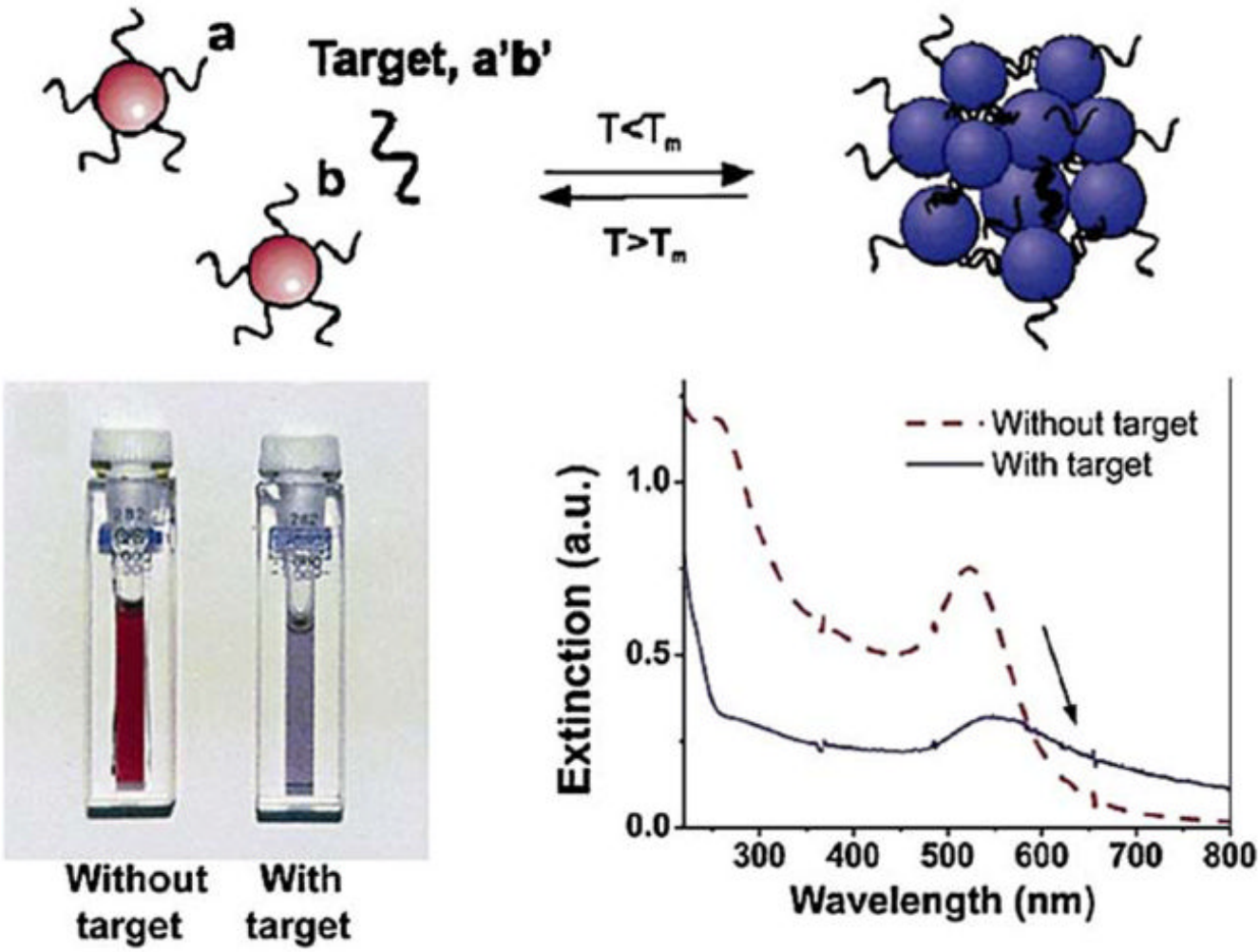

Figure 9.
Detection of the presence of a target sequence (a'b') using complementary DNA oligomers (a and b) bound to gold particles. From [44].

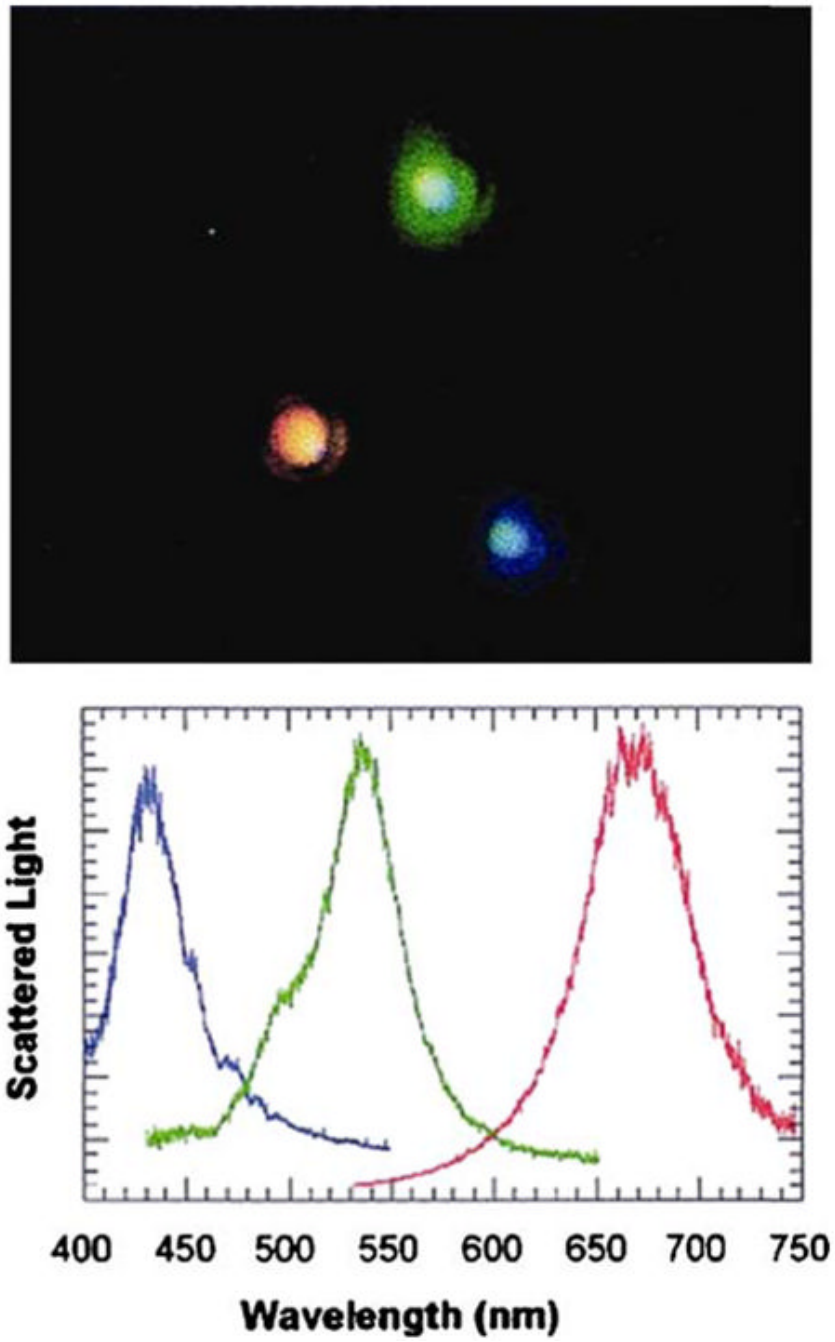

Figure 10.
Top, photograph of three different size colloids with white light epi-illumination. Bottom, Scattering spectra of the three colloids. From [46].

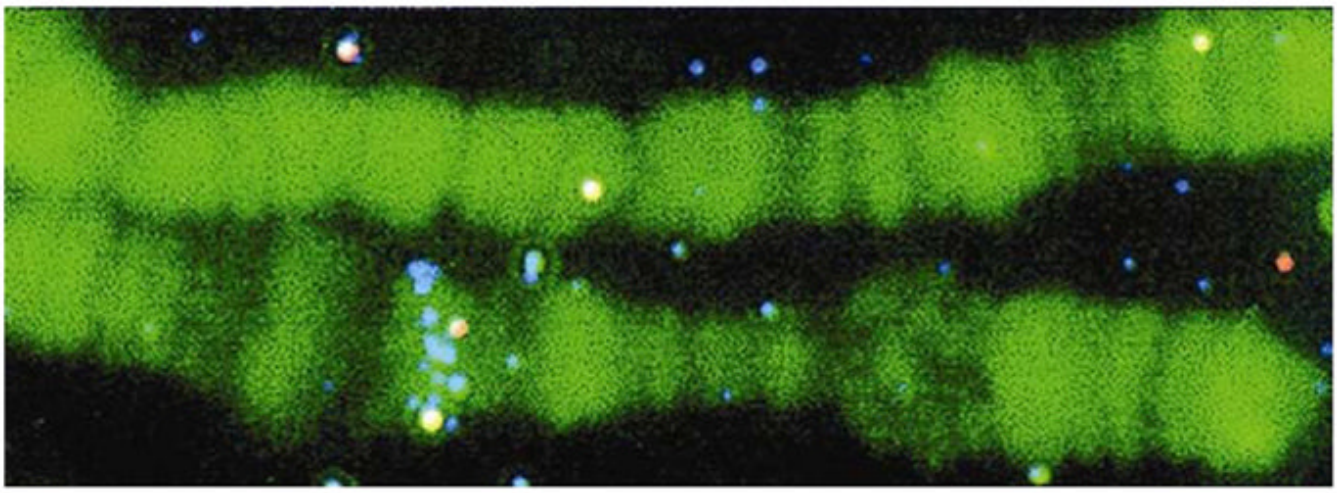

Figure 11.
Dark field image of a *Drosophila* polytene chromosome stained with SYBR Green. The bright spots are metal colloids bound to specific locations by hybridization. From [46].

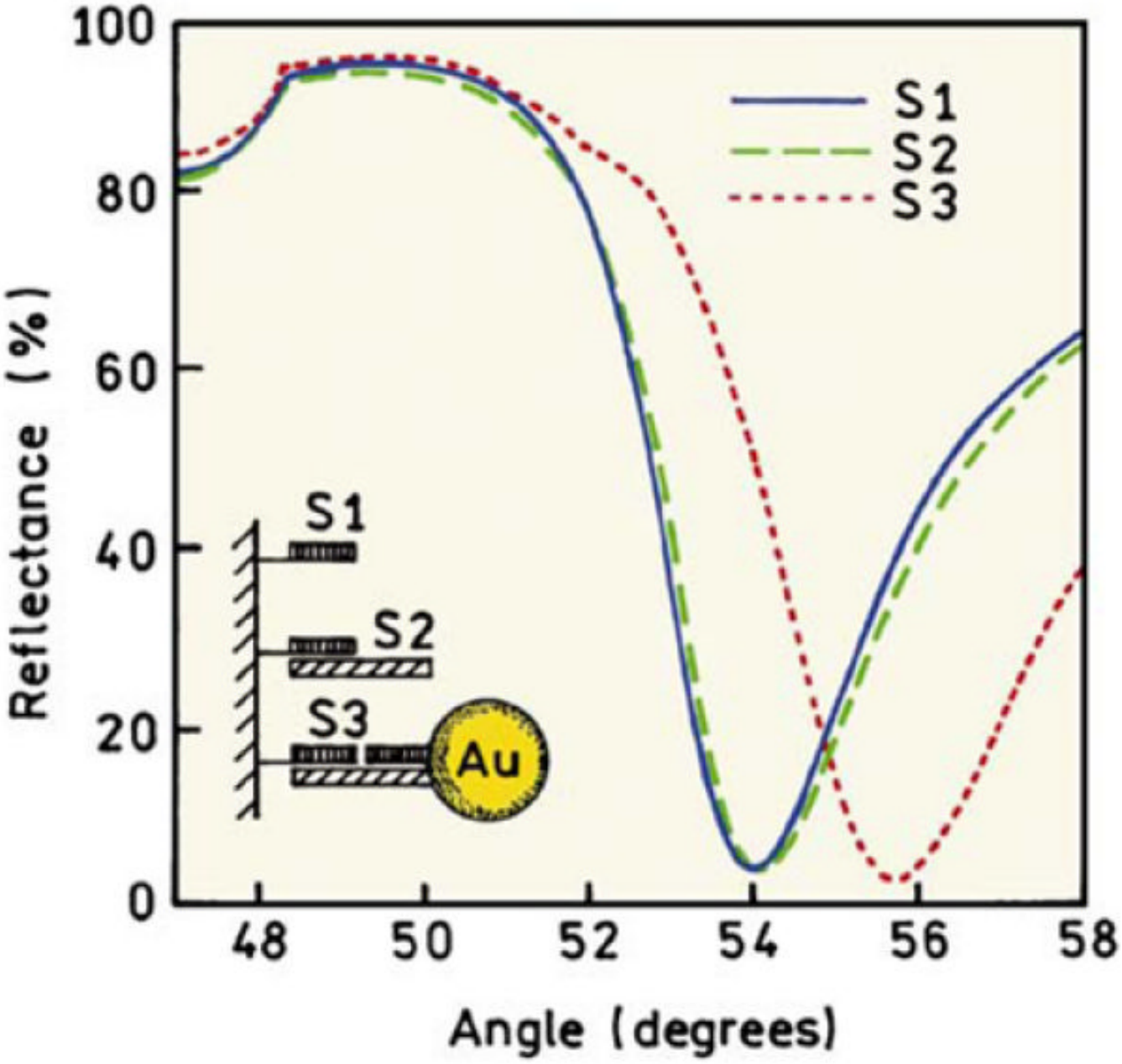

Figure 12.
SPR measurements of DNA hybridization without (S2) and with Au particle amplification (S3). Revised from [51].

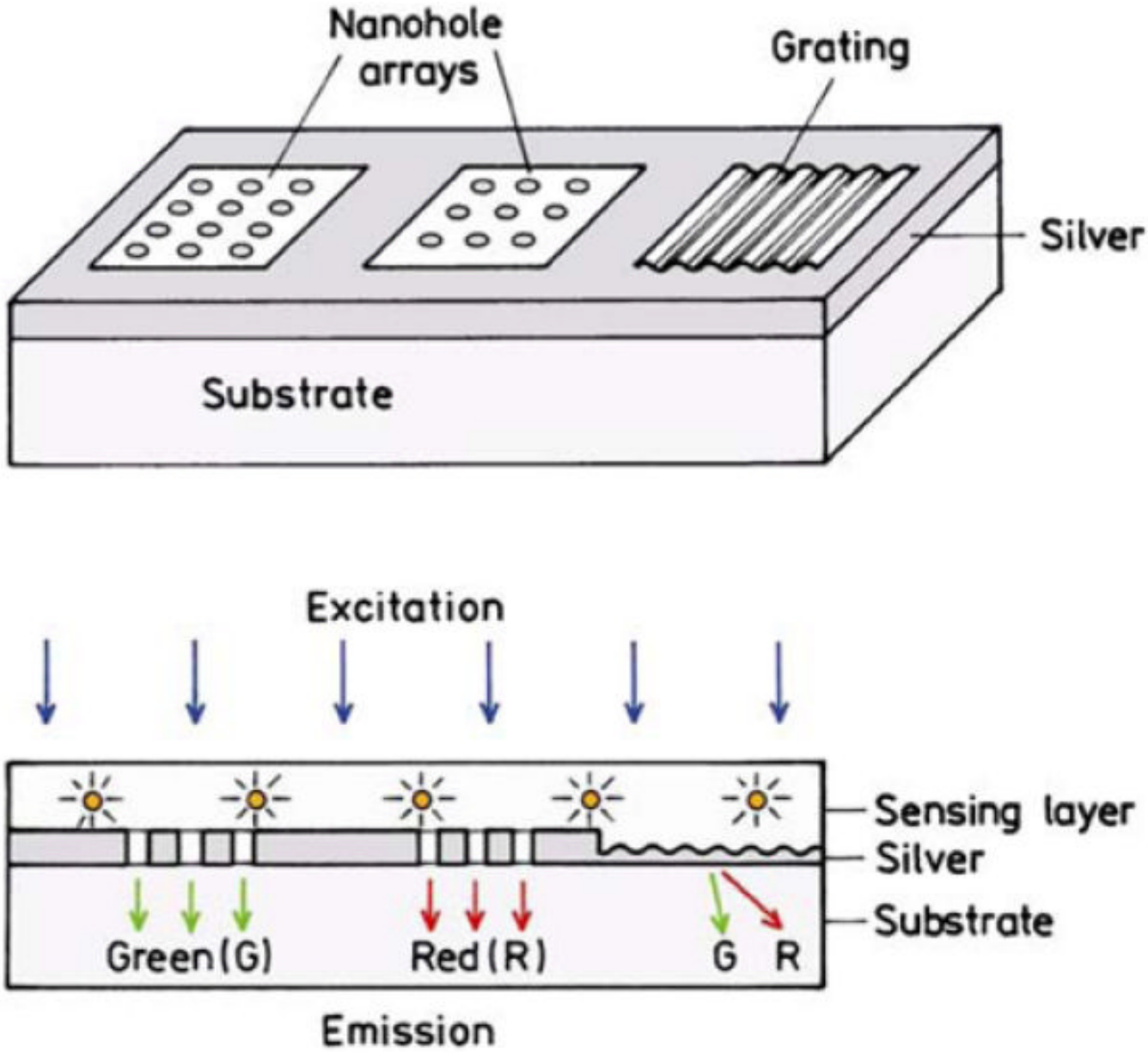

Figure 13.
Schematic of using PCF for sensing. The periodicity of the nanohole array is chosen to couple to green (G) or red (R) emitting fluorophores. The periodicity of the grating is appropriate for separating red and green wavelengths.

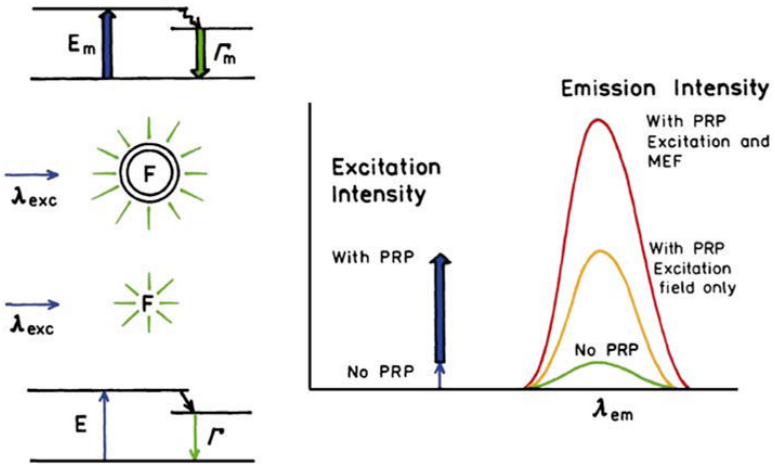

Figure 14.
Comparison of fluorescence with no PRPs, with the effect PRPs on the enhanced excitation field, and with the PRPs enhancing both excitation and emission.

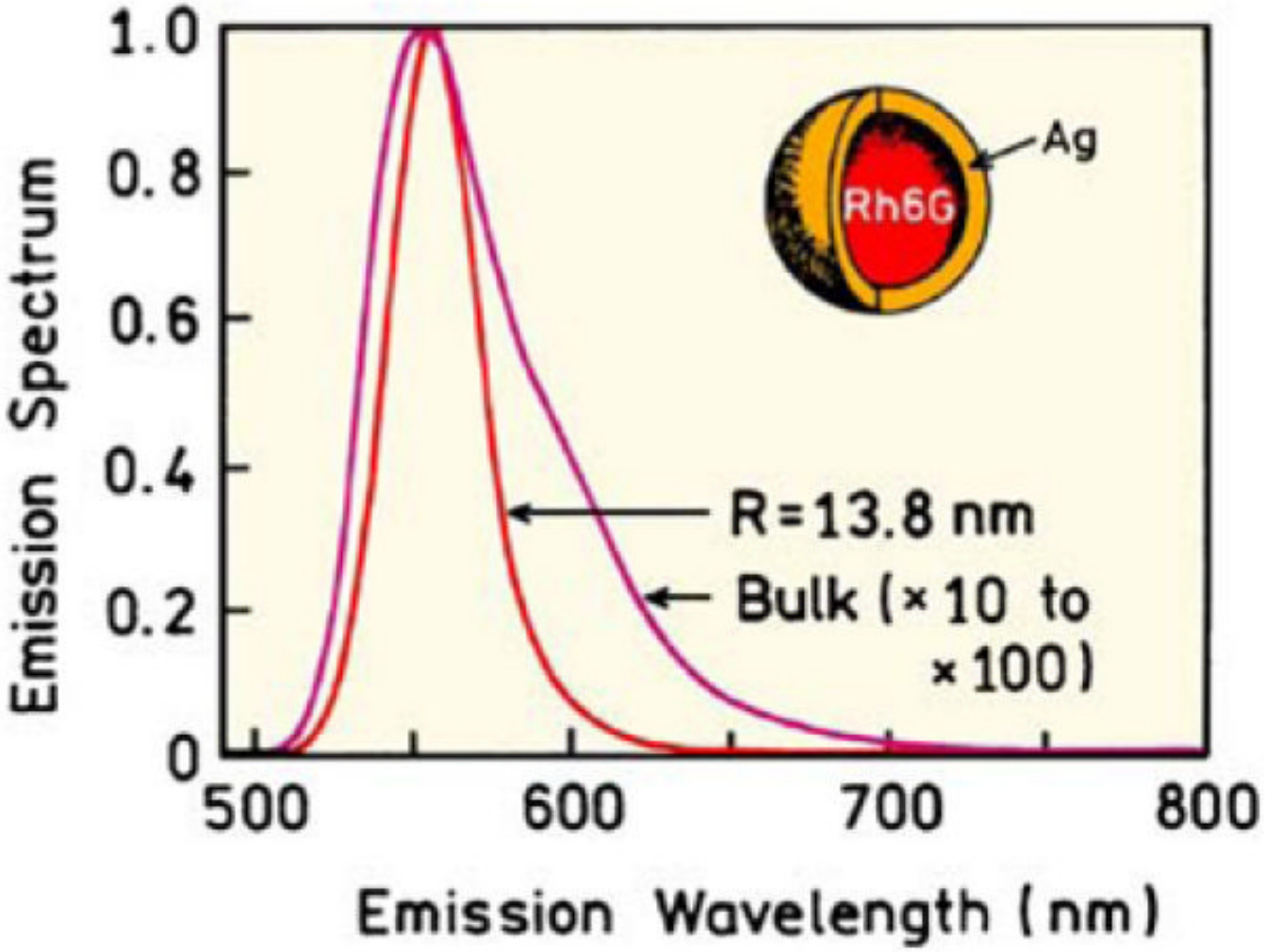

Figure 15.
Calculated intensities and emission spectra for Rh6G in a silver shell. From [52,53].

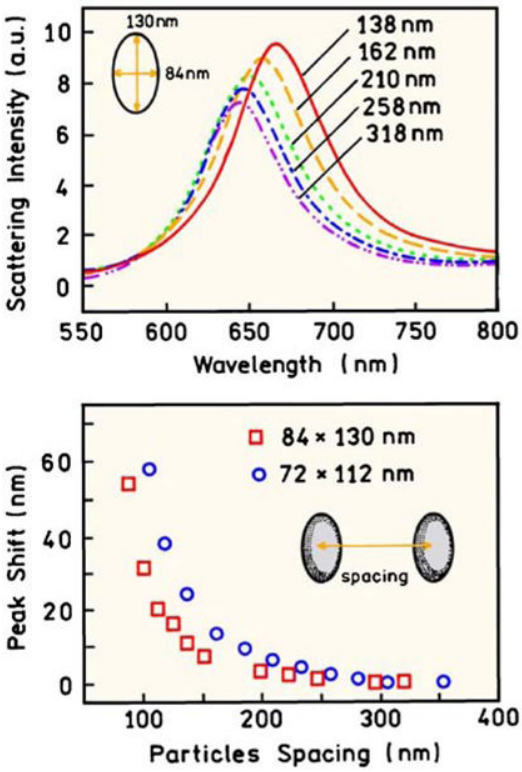

Figure 16.
Scattering spectra and peak scattering wavelengths calculated for two elliptical disks at varying center-to-center distances. Top, the numbers on the right indicate the particle center-to-center distances. Revised from [71].

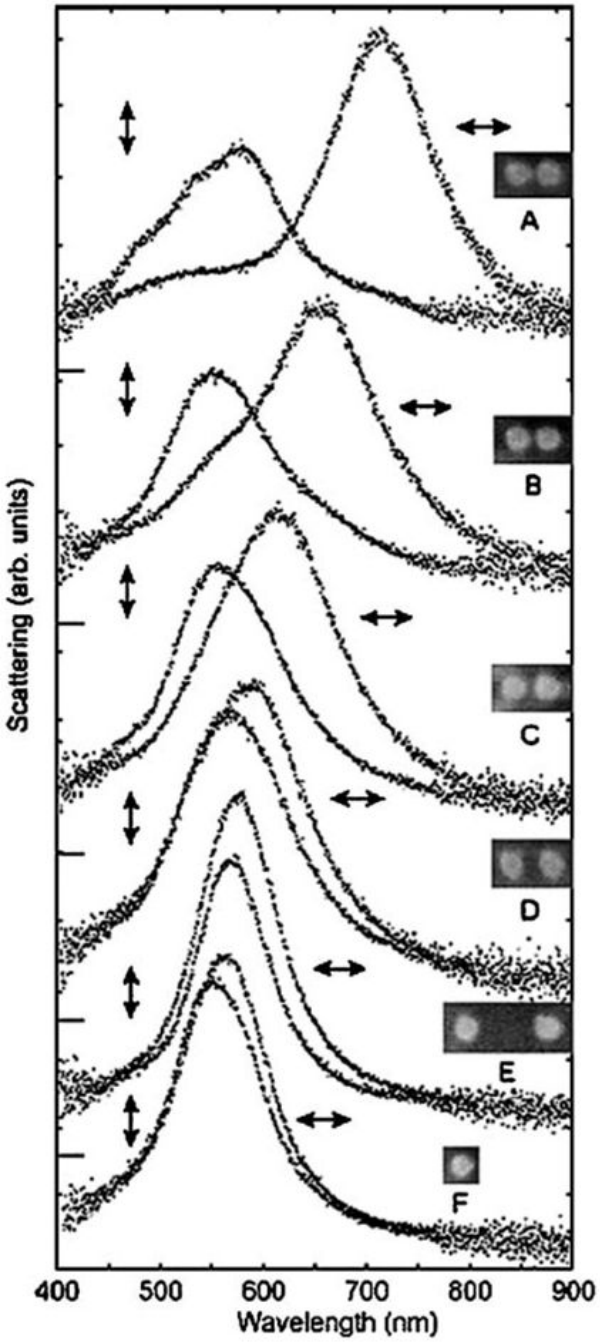

Figure 17.
Dark-field scattering spectra and scanning electron micrography of isolated disk-shaped particle pairs. The arrows indicate the polarization of the incident light. The gaps between the particles are approximately 10, 15, 25, 50, and 250 nm, for A through E. F is an isolated particle. The disks are about 95 nm in diameter and 25 nm high. From [72].

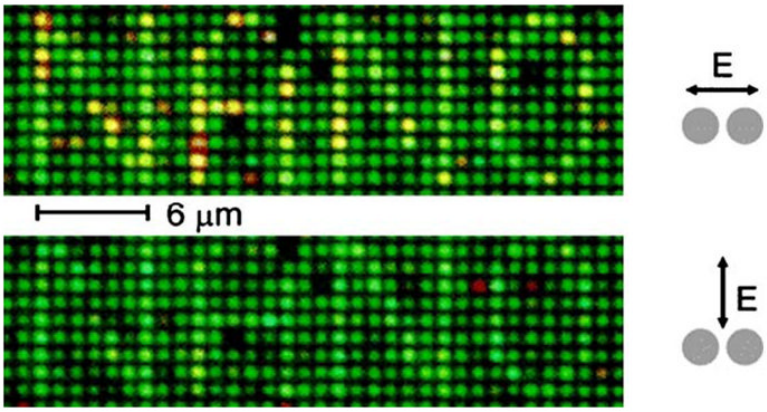

Figure 18.
Dark-field images of an array of silver particle pairs. The term NANO is written by single pairs of disk-shaped particles, 80 nm in diameter, 25 nm high, with a center-to-center distance of 110 nm. The other locations are occupied by single particles of the same size. From [72].

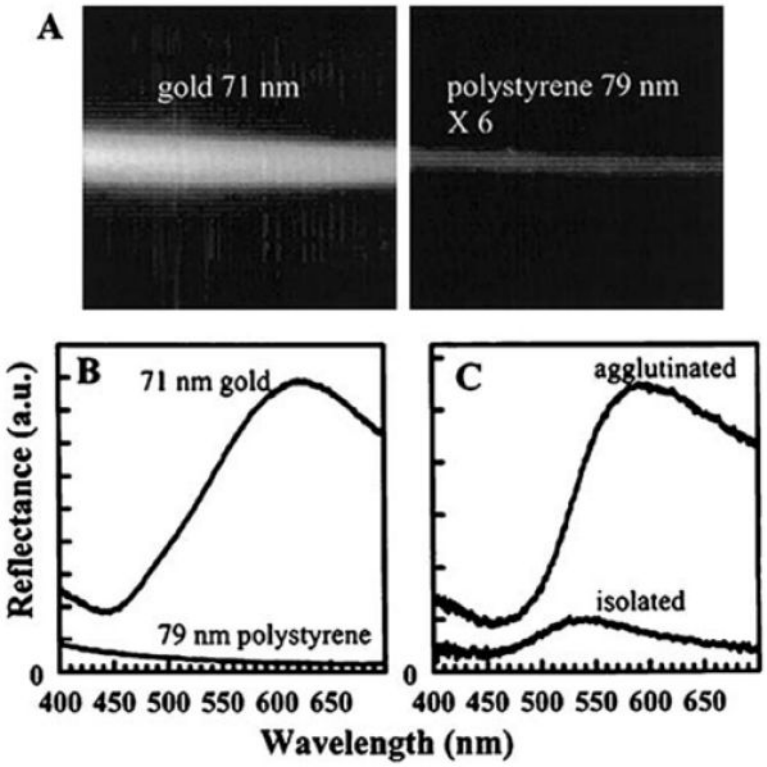

Figure 19.
(A and B) Comparison of the scattered light intensity (630-680 nm) from gold particles and 6-fold more concentrated polystyrene particles. (C) Comparison of the scattering spectra of isolated and clustered gold particles. From [73].

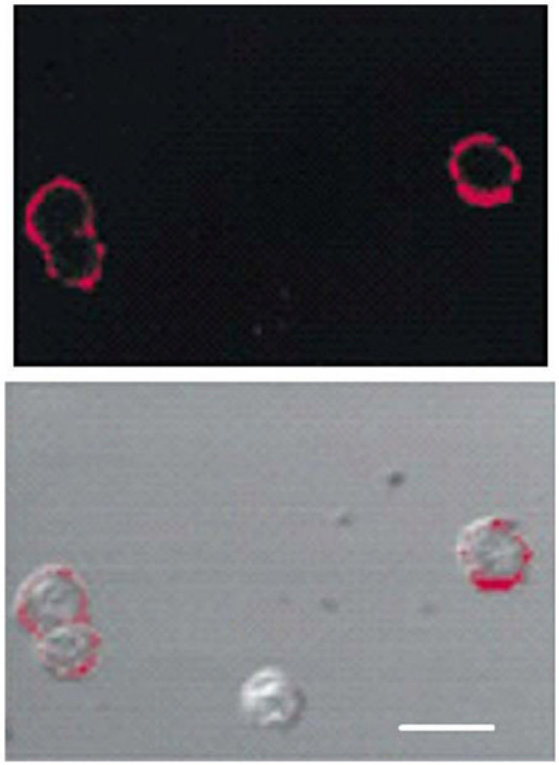

Figure 20.
Top, laser scanning confocal reflectance images of cervical epithelial cancer cells with gold colloids targeted to the GFR. Illumination at 620-680 nm. Bottom, overlay of the reflectance image with the transmitted light image. Scale bar is 30 μm. From [73].

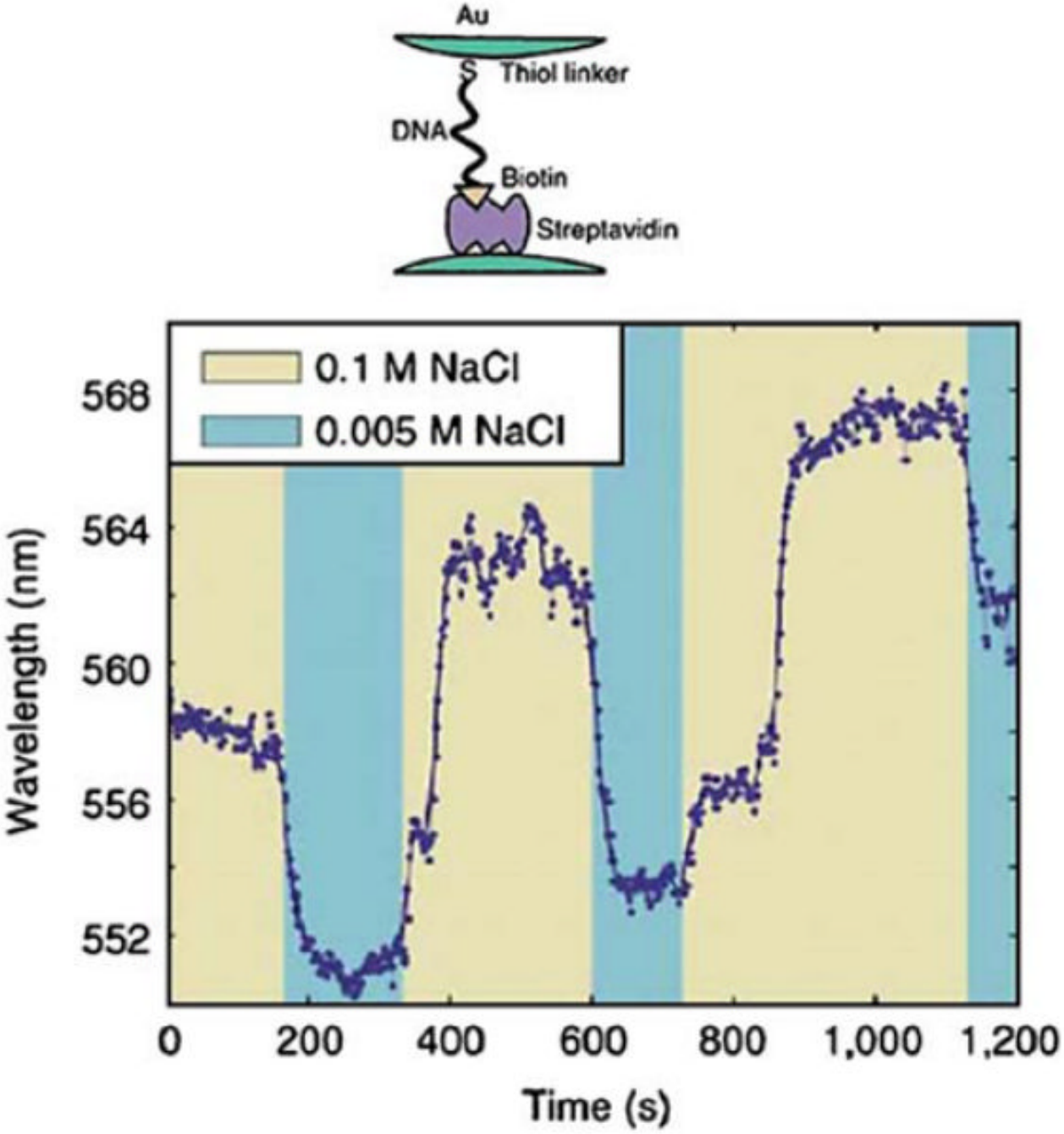

Figure 21.
Effect of ionic strength on the peak scattering wavelength of gold colloids linked by DNA and streptavidin. From [74].

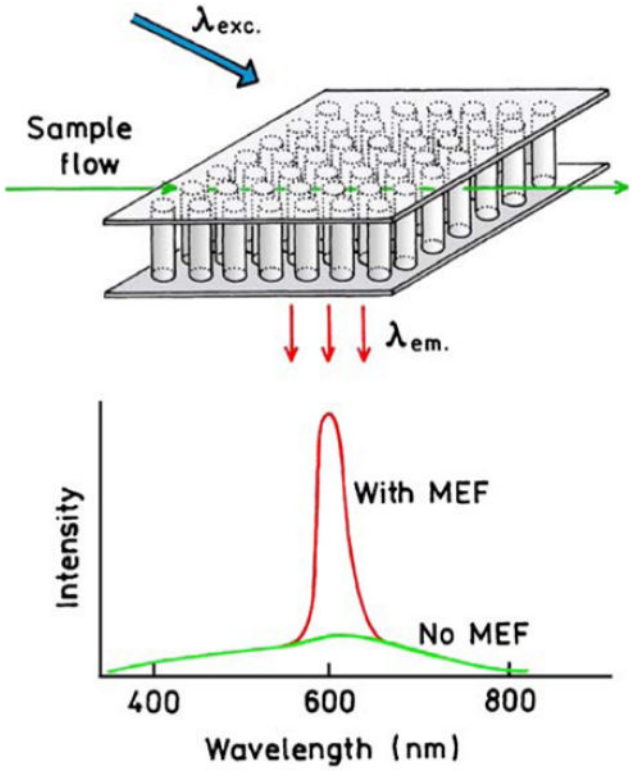

Figure 22.
Schematic of wavelength-selective enhanced fluorescence in the presence of background. Top, represents an array of metal nanowires spanning the top and bottom of a flow cell.

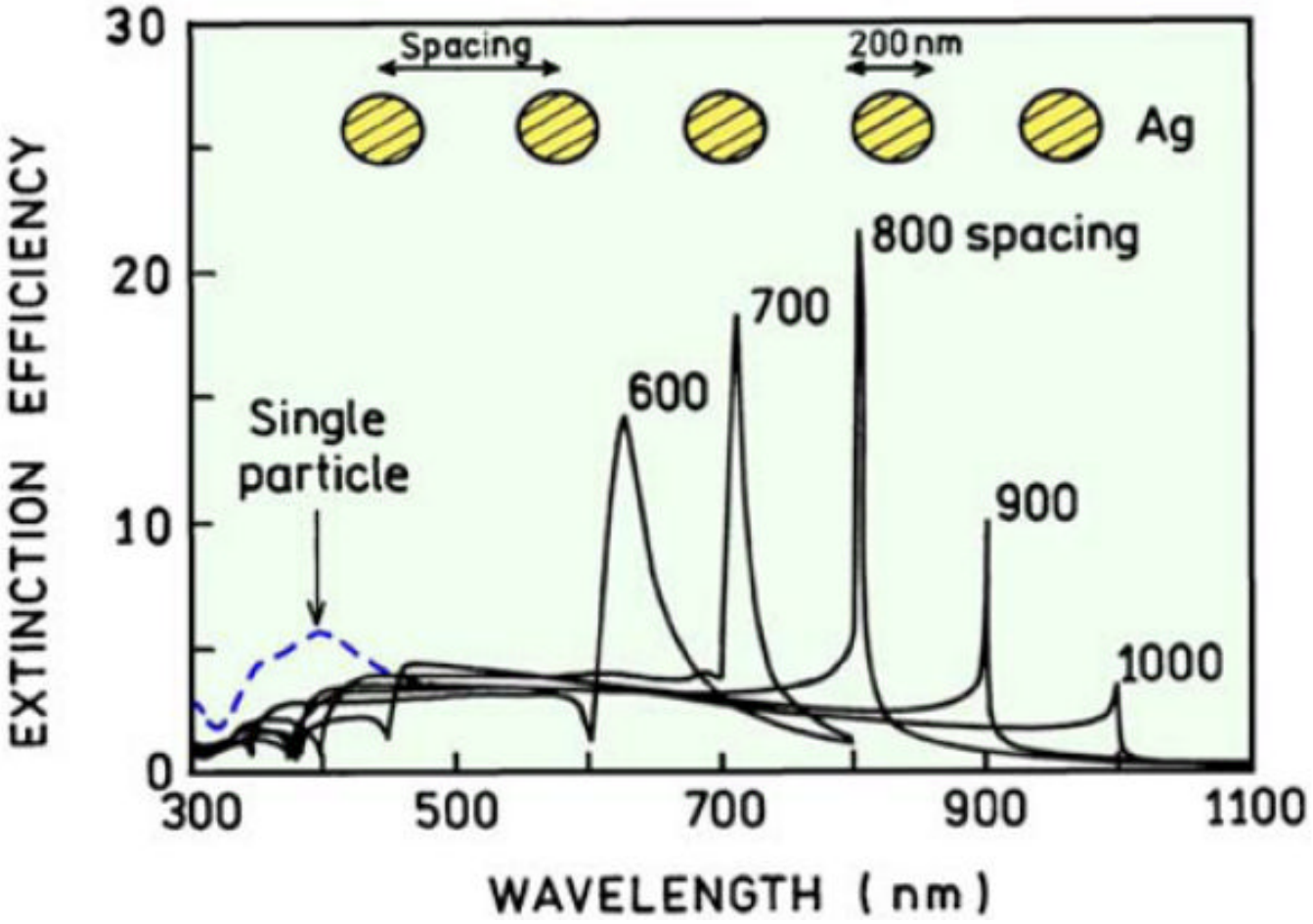

Figure 23.
Extinction spectra for a one-dimensional chain of silver nanoparticles. Revised from [82].

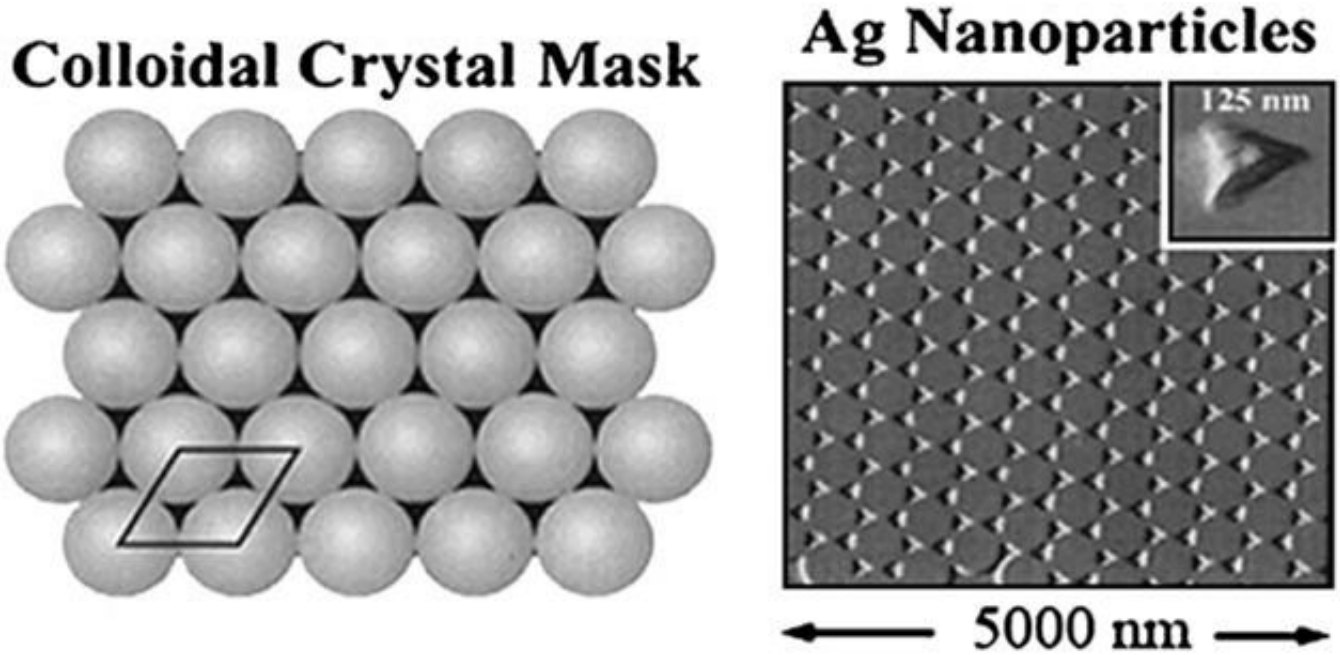

Figure 24.
Schematic of a colloidal mask and electron micrograph of nanotriangles prepared by NSL. From [84].

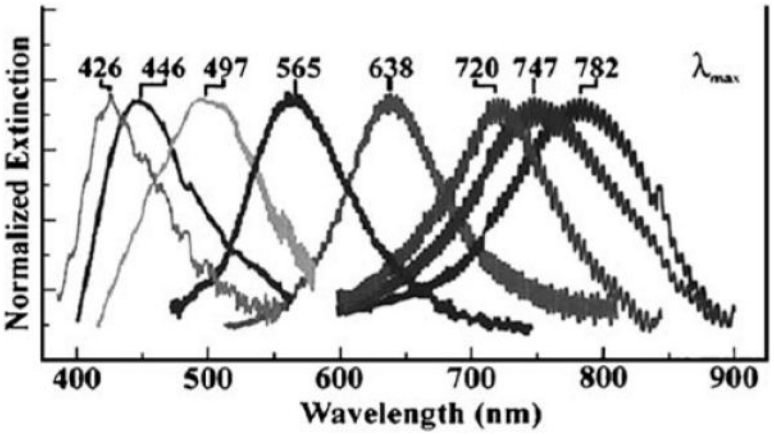

Figure 25.
Extinction spectra of silver particles prepared by NSL. The oscillations in the spectra are due to the apparatus, not the particles. From [86].

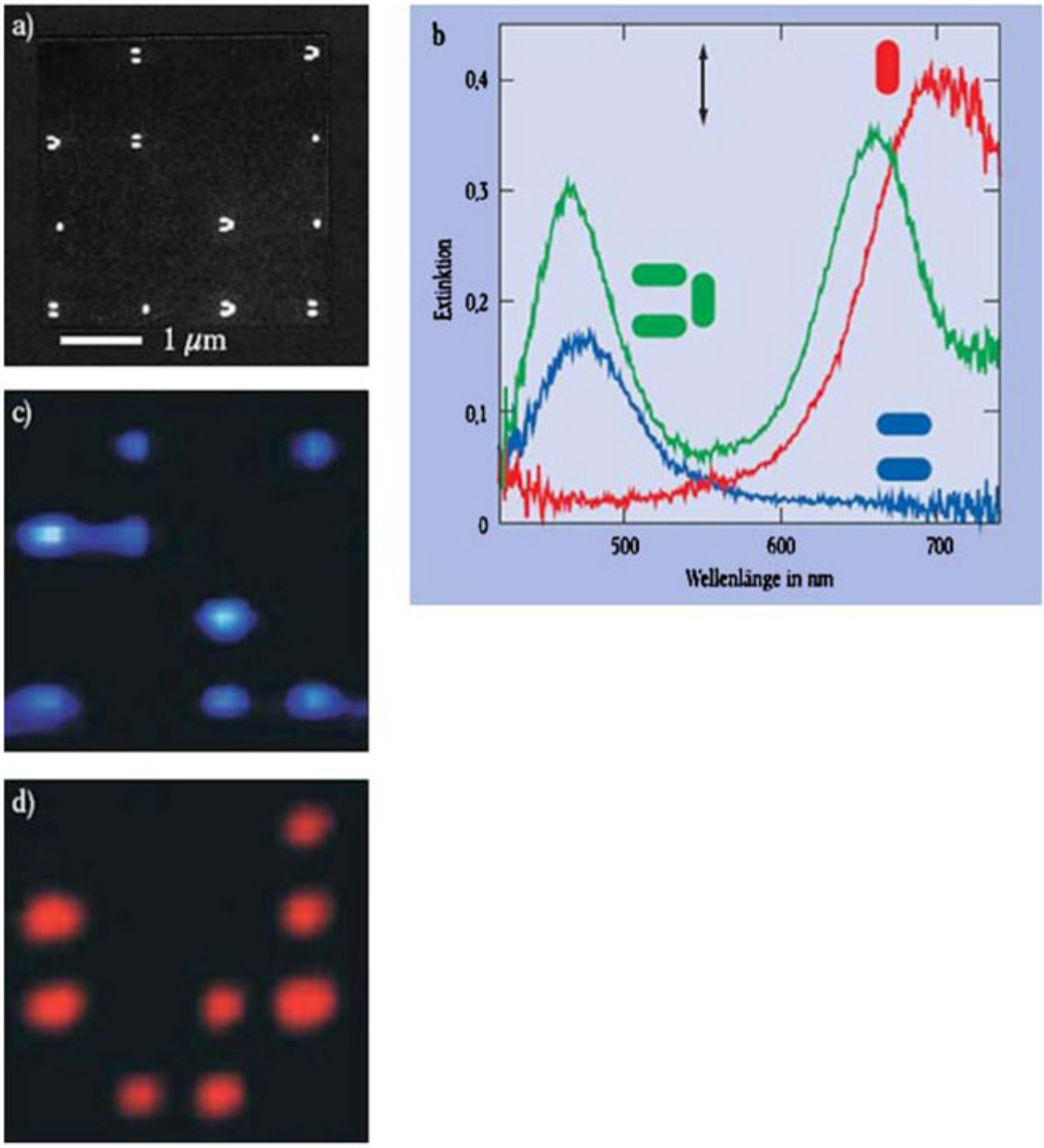

Figure 26.
Electron micrograph, photographs of scattered light, and scattering spectra of clusters of silver particles. The arrow shows the direction of the incident polarization. From [87].

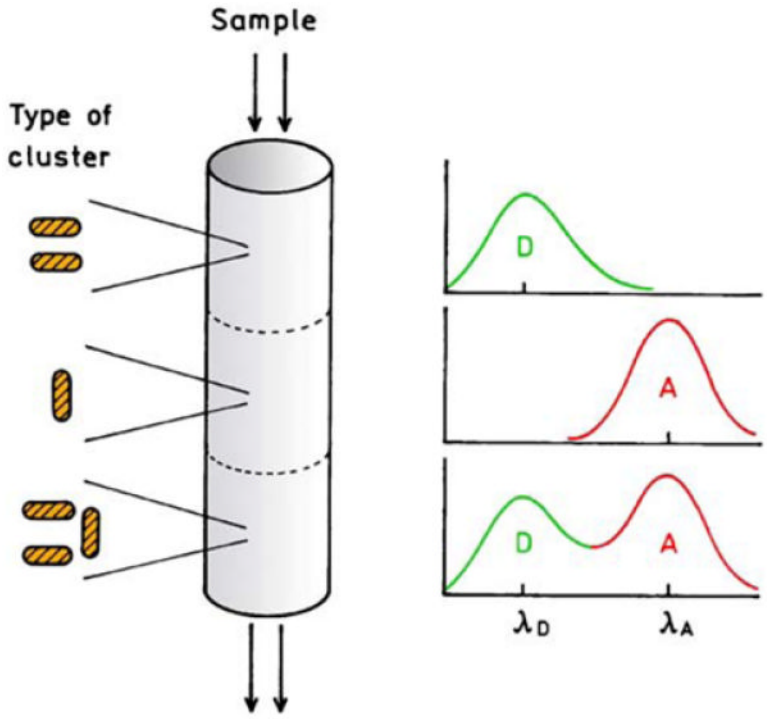

Figure 27.
Schematic of a plasmonic structure for wavelength-selective enhancement based on particle cluster.

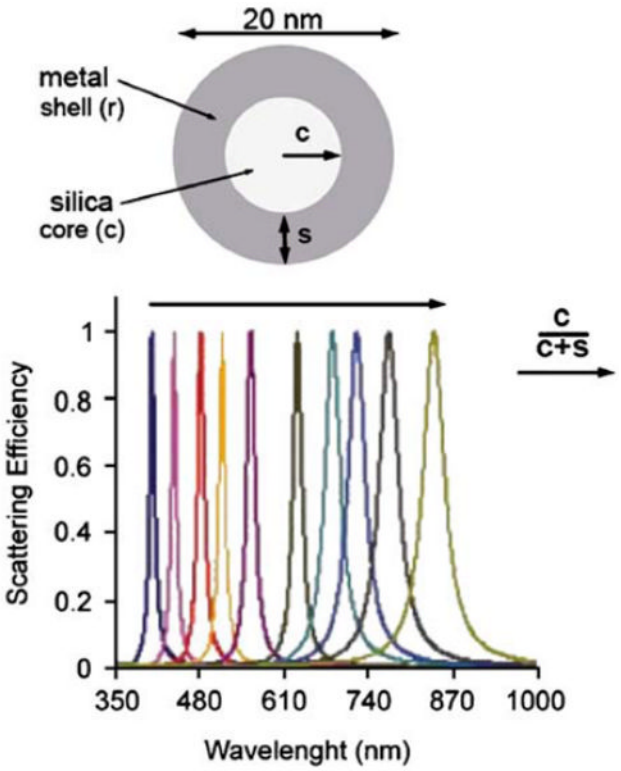

Figure 28.
Normalized scattering efficiency calculated for metal nanoshells on silica cores. Revised from [96].

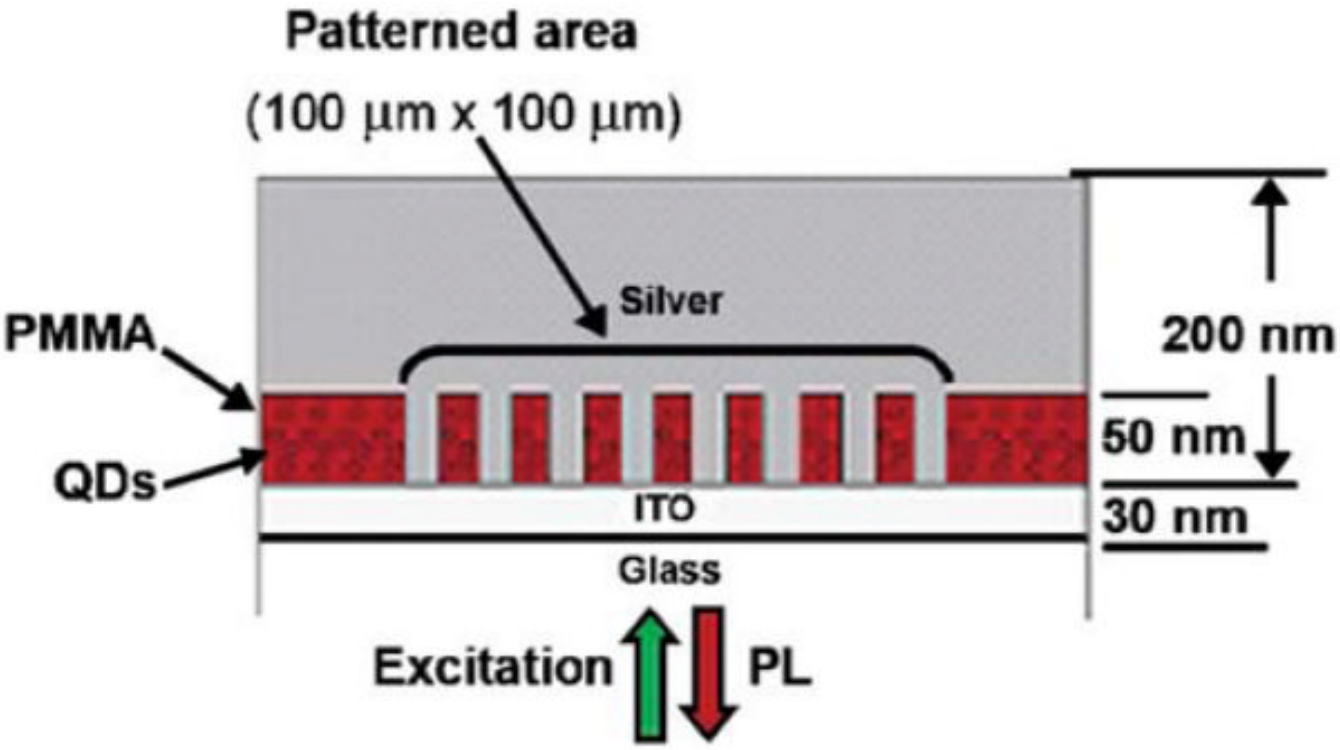

Figure 29.
Schematic of silver posts in PMMA containing Qdots. From [97].

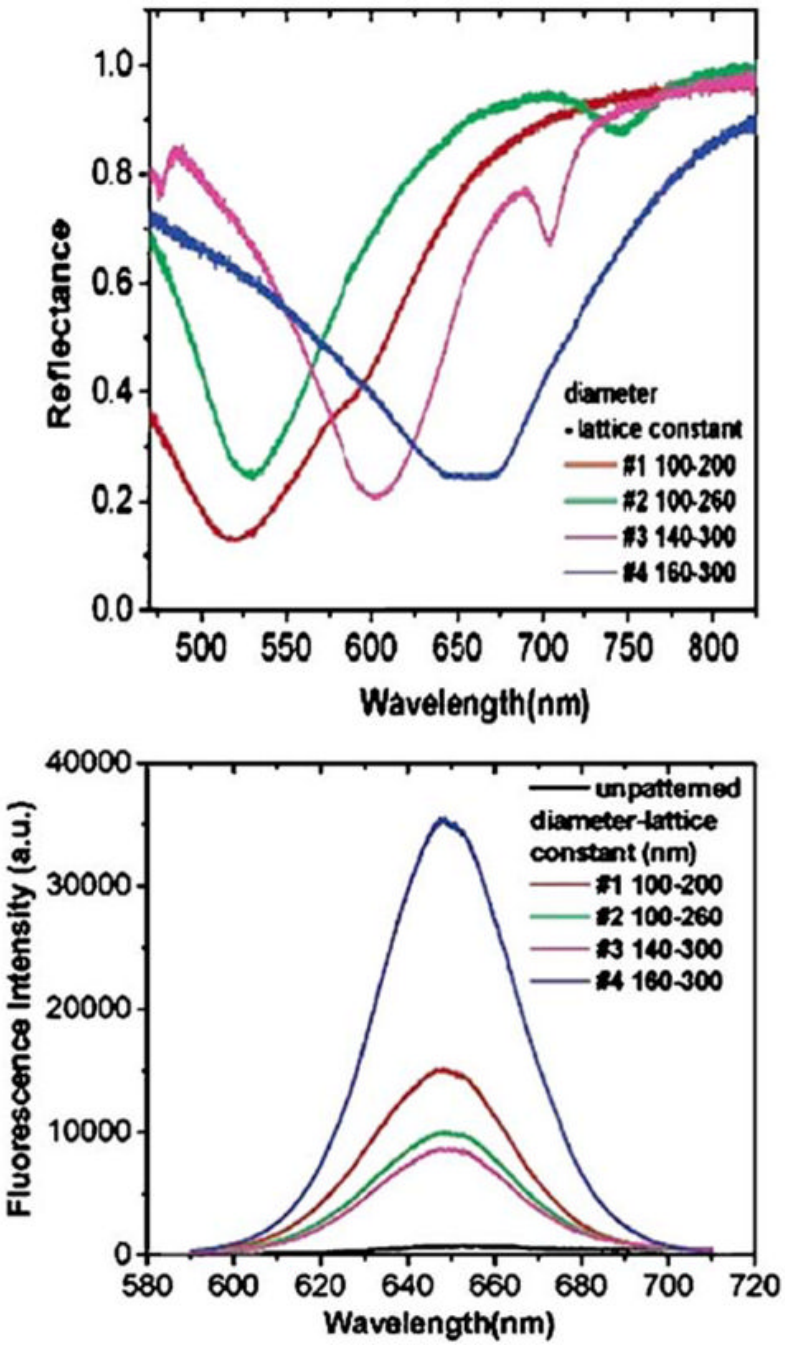

Figure 30.
Reflections spectra of the structured silver film (top) and emission spectra of the PMMA-embedded Qdots (bottom). Revised from [97].

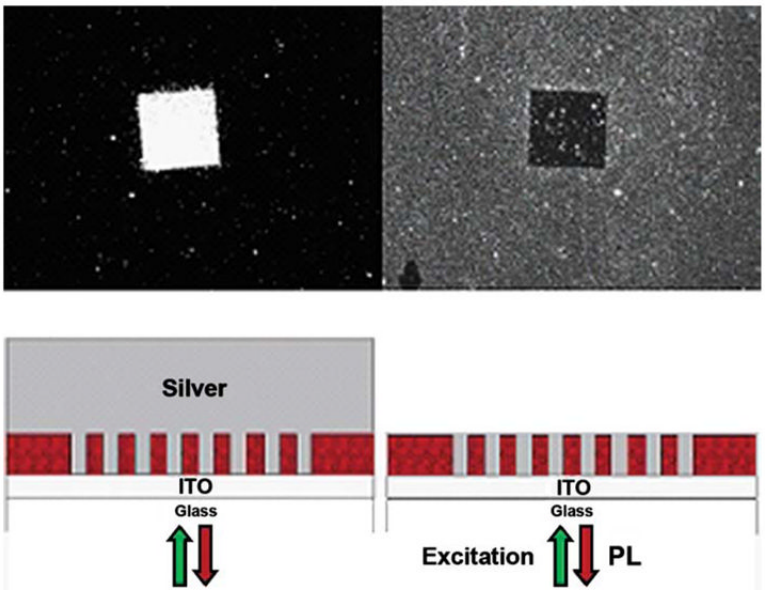

Figure 31.
Fluorescence images from the Qdots on the structure shown below. From [97].

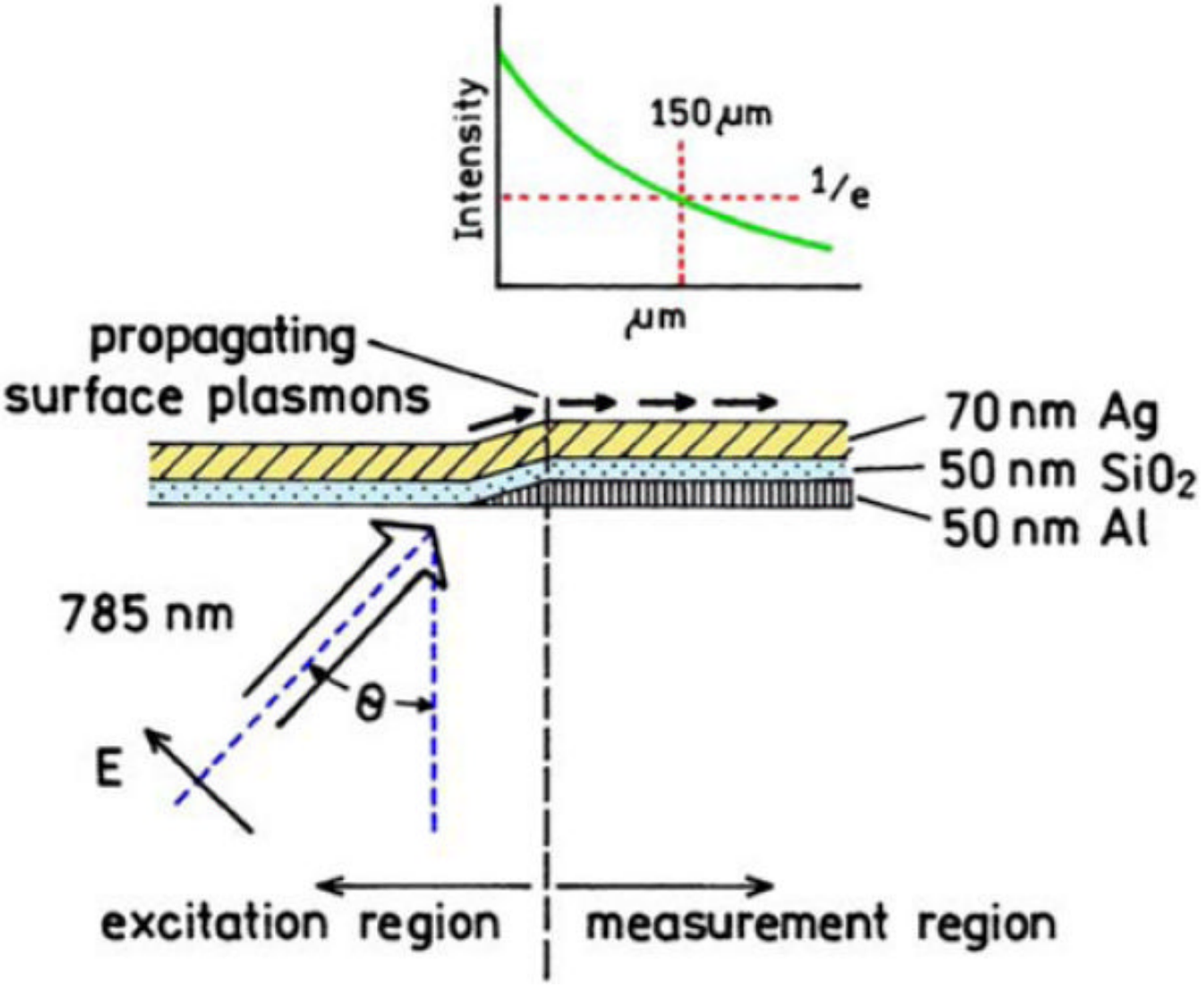

Figure 32.
Experimental setup to measure the distance of plasmon propagation in a metal film. Revised from [108].

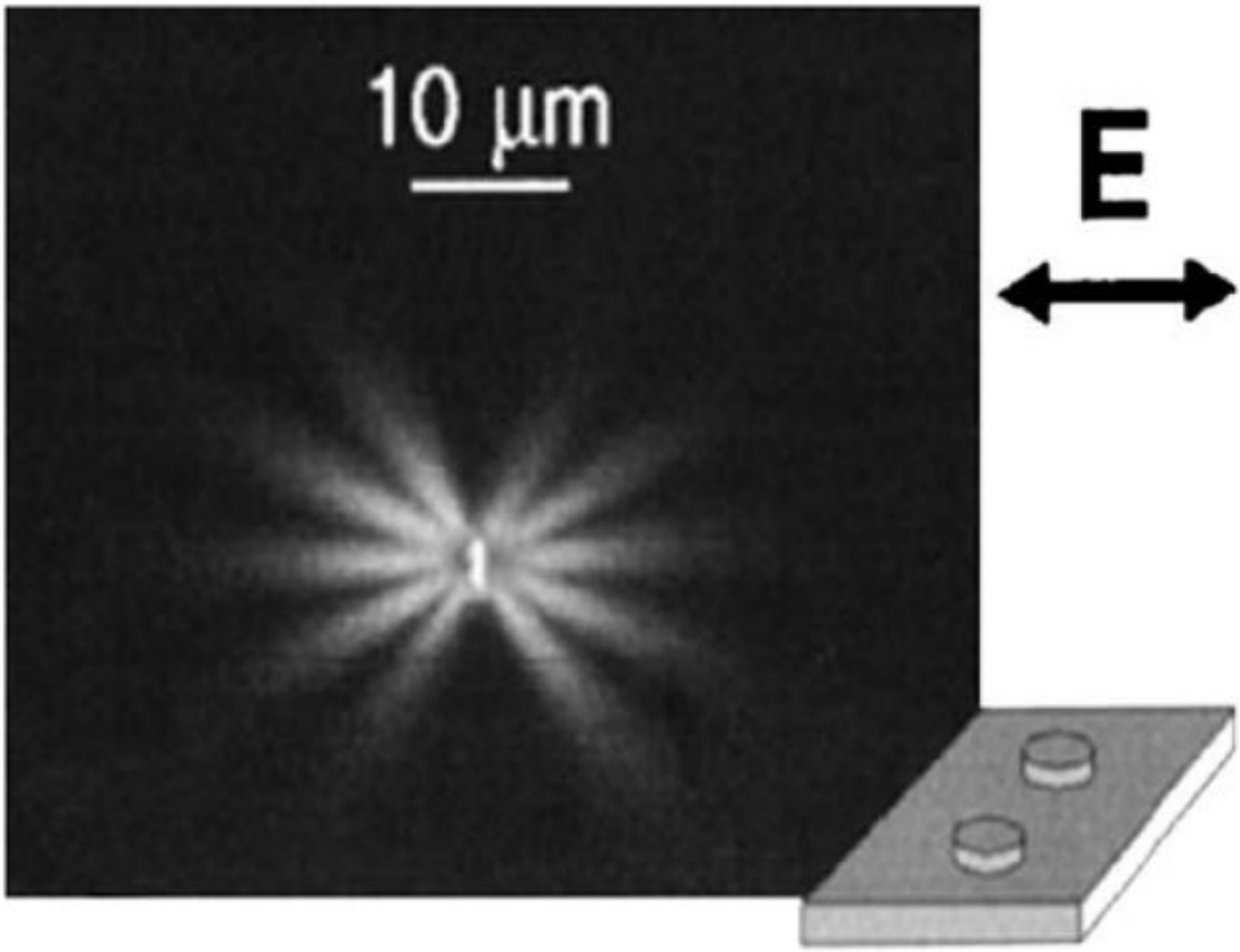

Figure 33.
Fluorescence image of plasmons created by illumination of a silver wire on silver film. The two metal surfaces were separated by 10 nm of silica. From [109].

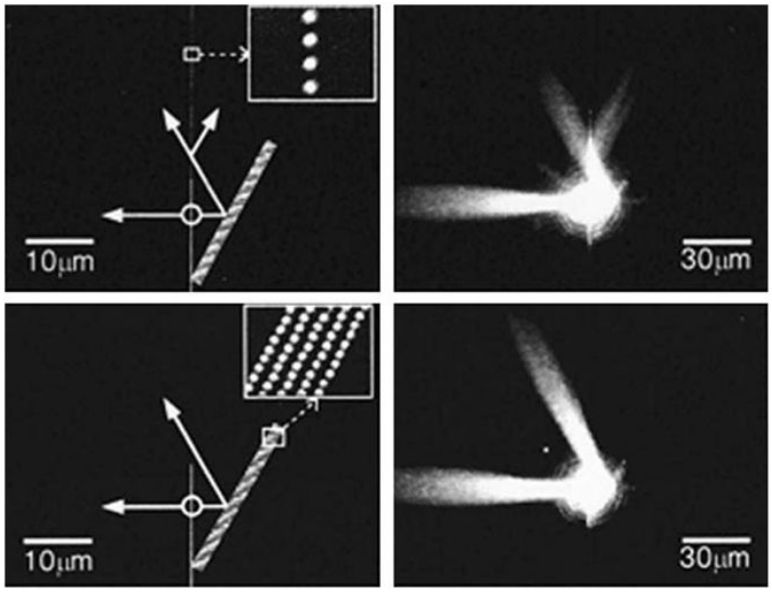

Figure 34.
Optical elements for surface plasmons using bumps on a silver film. Left: SEM images of the mirror (bottom) and mirror with beam splitters (top). Right: surface plasmons. From [111].

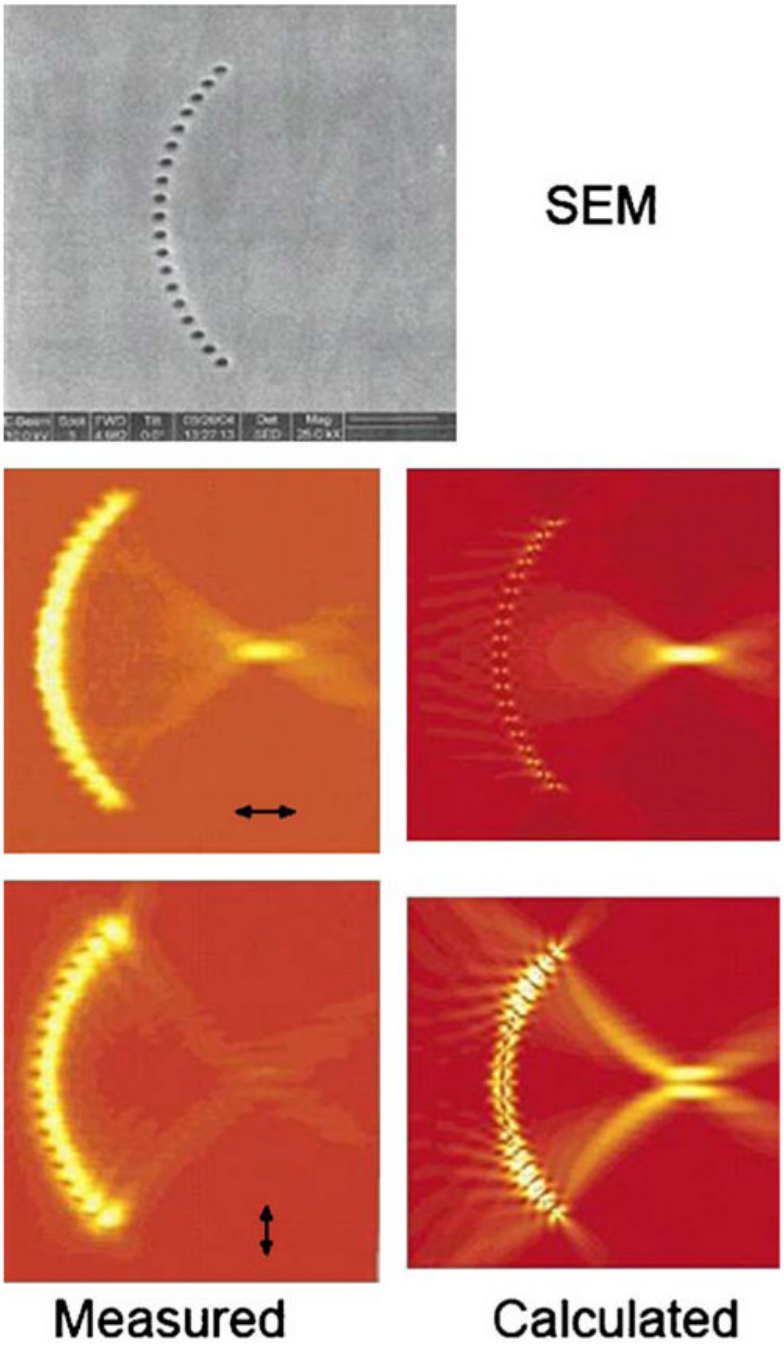

Figure 35.
Top, scanning electron micrograph of a semicircle of 200-nm holes in a 50-nm-thick film. Bottom, NSOM images (left) and calculated intensities (right) for the plasmon lines illuminated at 532 nm. From [113].

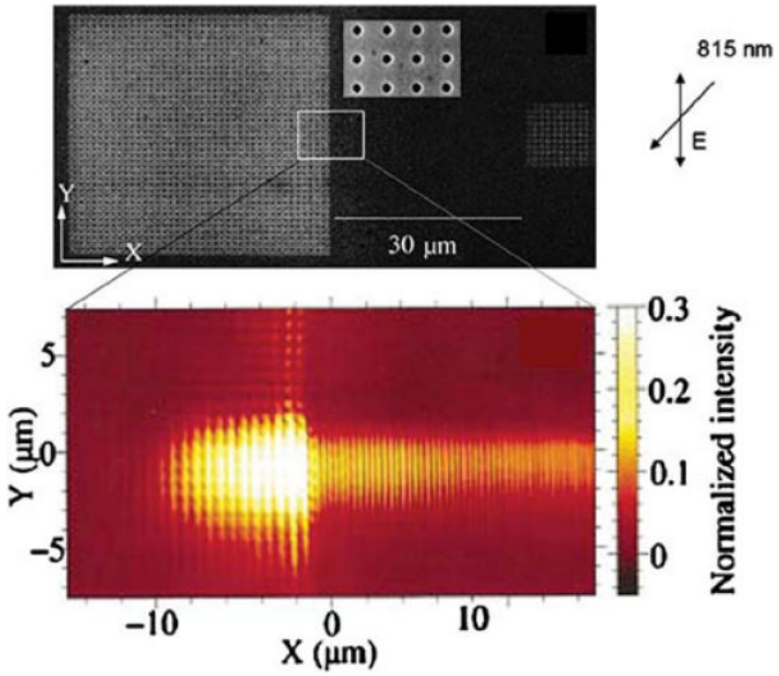

Figure 36.
Top, SEM image of the nanohole arrays on 150-nm-thick gold film. The array on the left is 41×41, and the array on the right is 11×11. Bottom, near-field image of the central region of the top panel. Revised from [110].

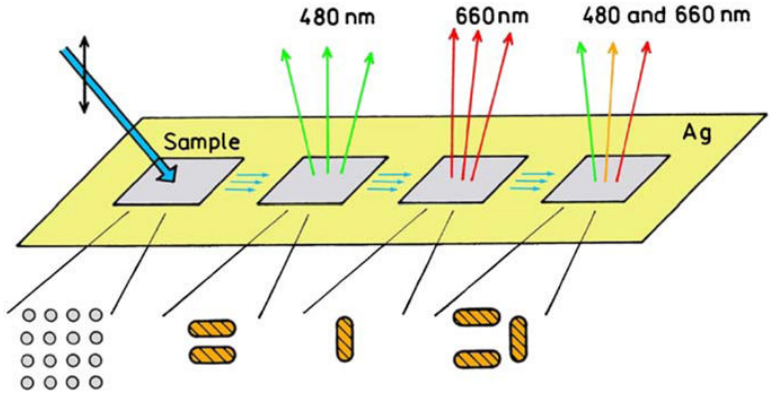

Figure 37.
Possible configuration of a sensor using plasmon engineering.

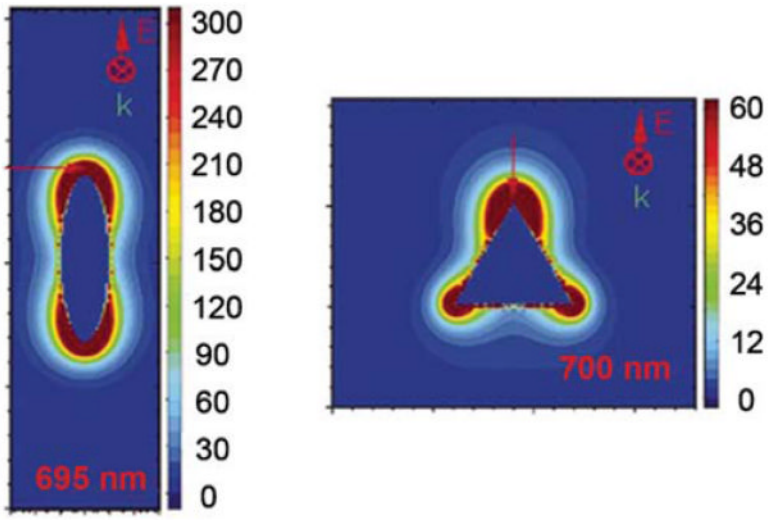

Figure 38.
Field enhancements around the silver particles calculated using the discrete dipole approximations. The maximum enhancement for the ellipsoid is 4700 and for the triangle is 3500. From [116].

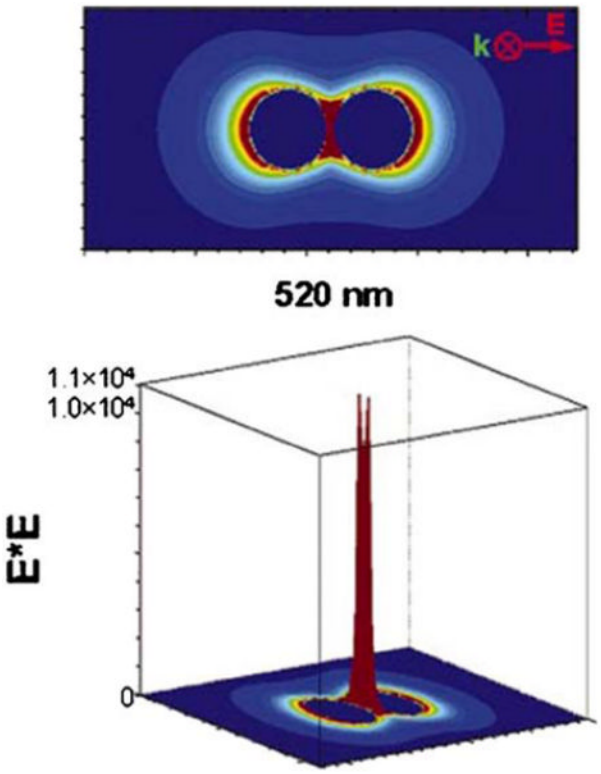

Figure 39.
Calculated field enhancement bear two closely spaced silver particles. The particles are separated by 2 nm. From [116].

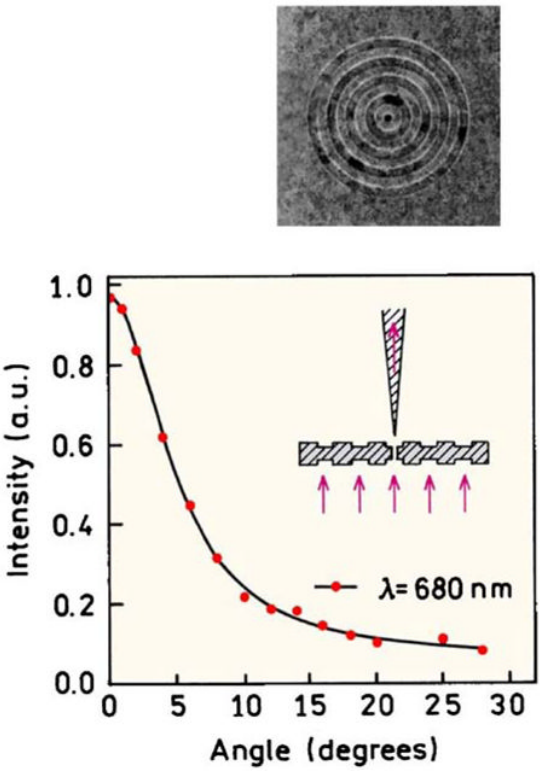

Figure 40.
Top, focused ion beam micrograph of a silver film, 300 nm thick, 350-nm hole diameter, 500-nm periodicity with 60-nm-deep groves. Bottom, angular distribution of transmitted light at 660 nm. Revised from [127].

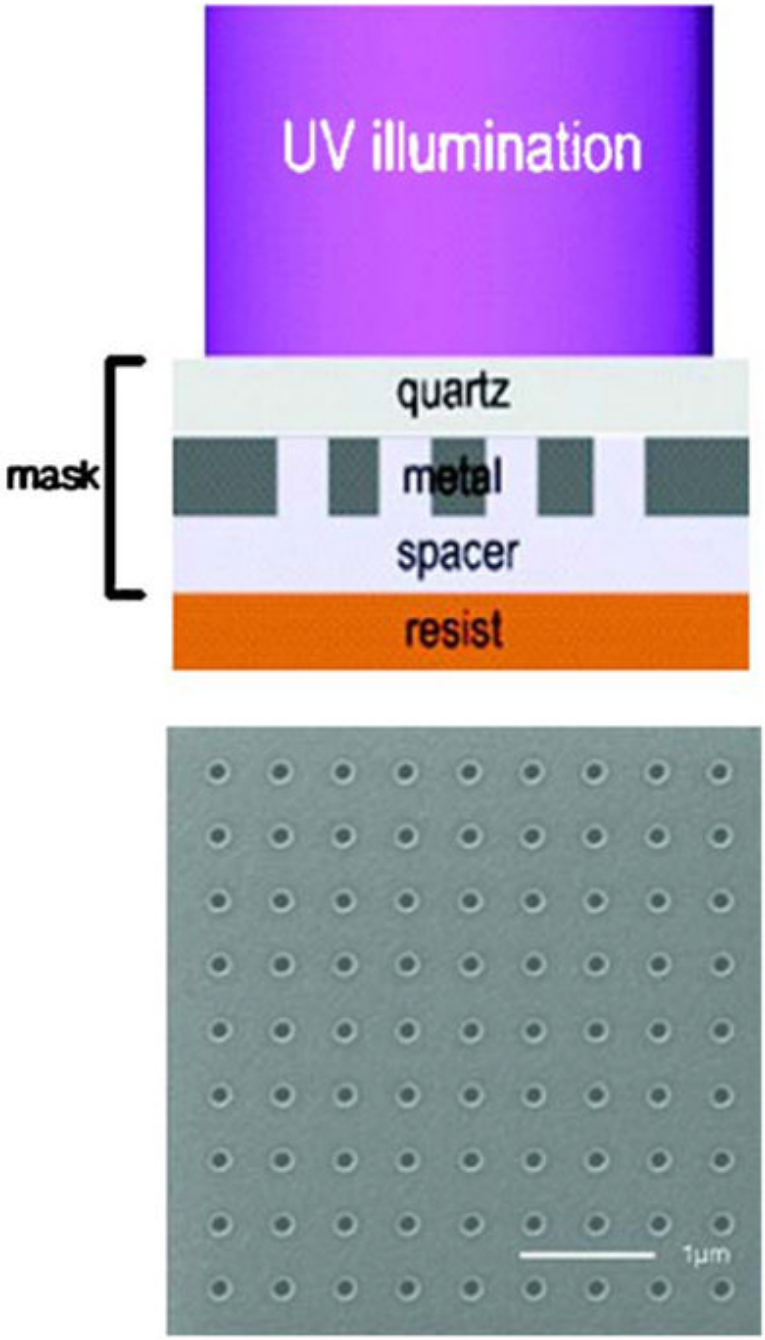

Figure 41.
Top, schematic of the surface plasmon optical lithography. Bottom, focused ion beam image of a hole array mask with hole size of 160 nm and period of 500 nm. From [131].

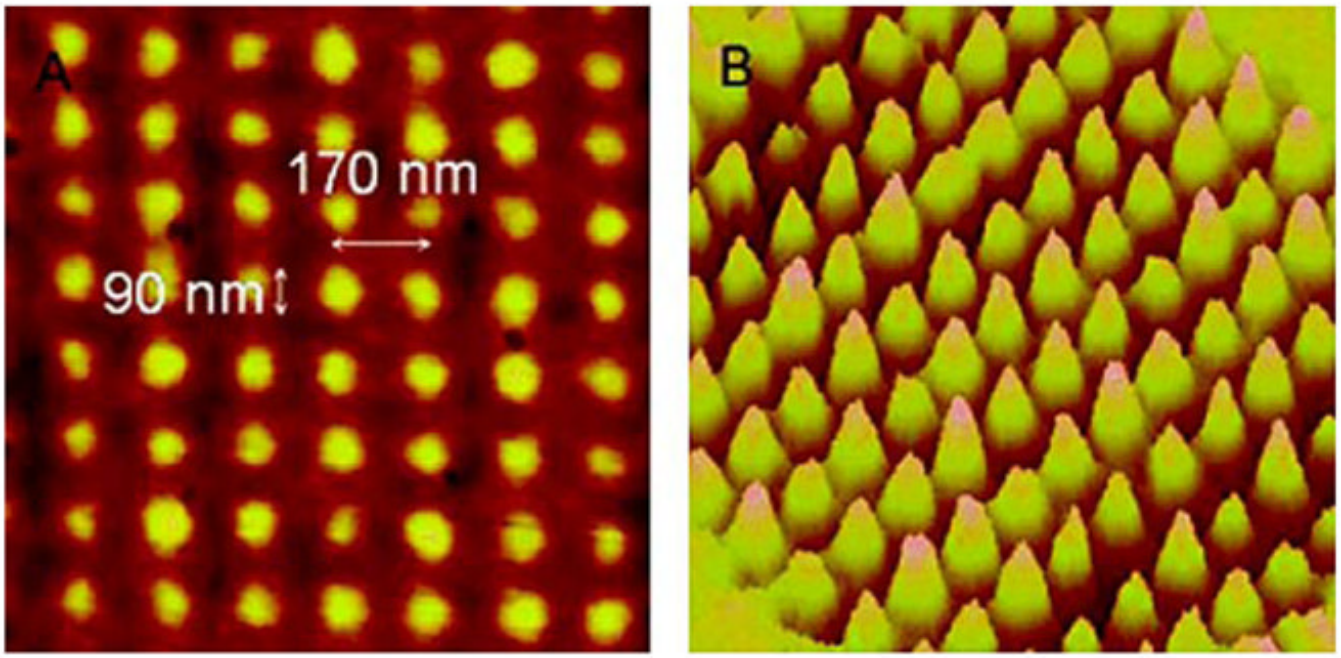

Figure 42.
AFM image of a pattern with 90-nm features with a period of 170 nm prepared by surface plasmon lithography (left) and 3D image of this structure (right). From [131].

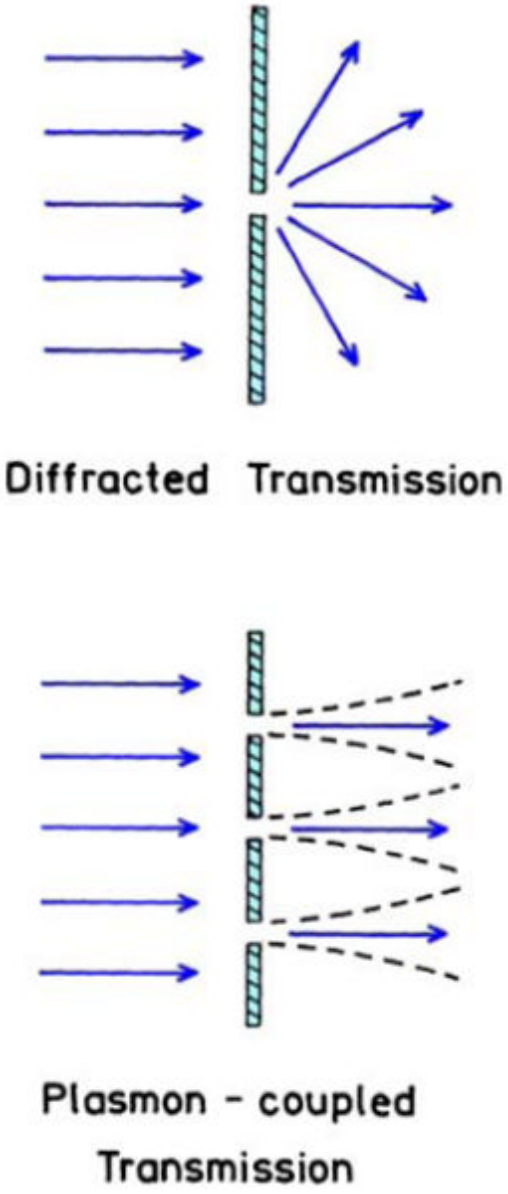

Figure 43.
Transmission through nanoholes in a metal film.

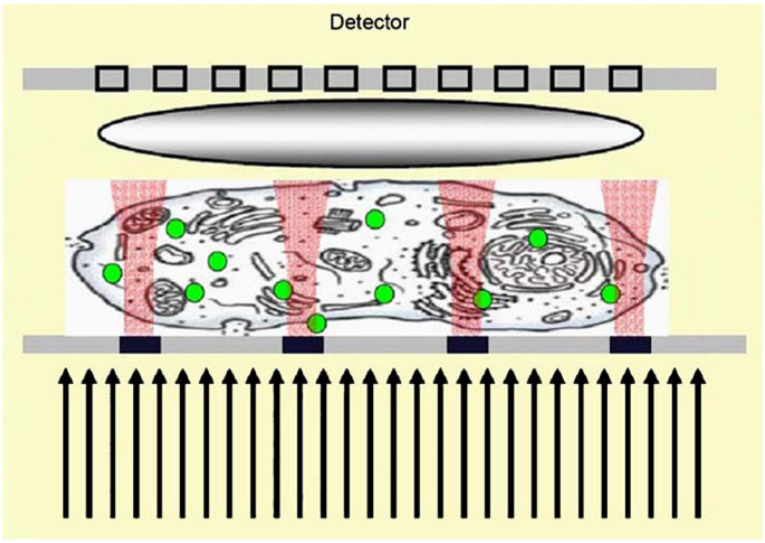

Figure 44.
Possible schematic for a subwavelength plasmonic microscope. Revised from [135].

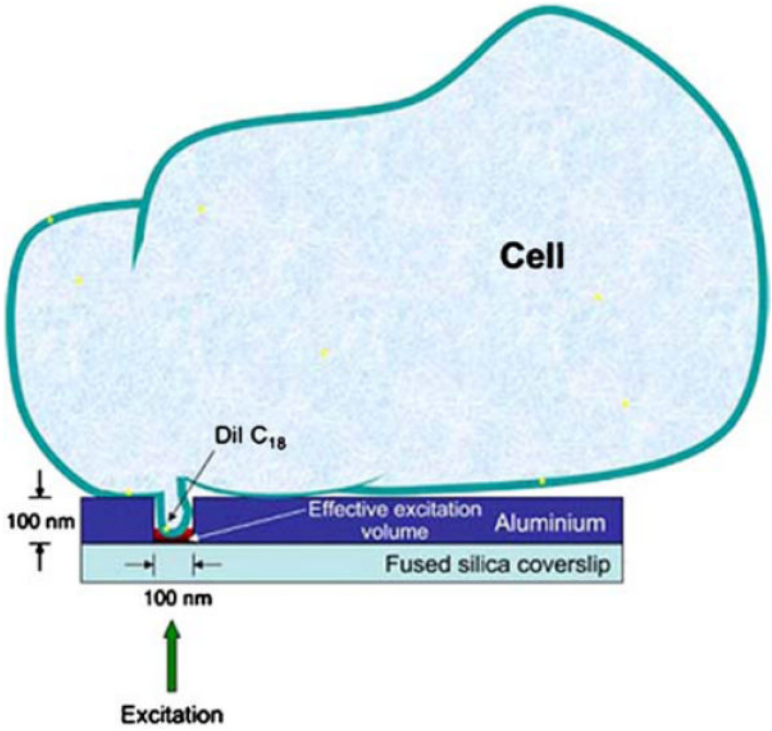

Figure 45.
Experimental arrangement used to obtain excitation of a 100-nm region of a cell membrane. An incident field is present only at the bottom of the hole in the aluminum film. From [137].

Table I

Optical properties of fluorophores, Qdots, and metal colloids

Substance/Diameter	ε (M^{-1} cm^{-1})	C (cm^2)	($c/\pi r^2$)	Q (Quantum yield)	Relative brightness
Fluorescein, 5 Å	72,000	2.75×10^{-16}	0.14	≈0.5	0.002
Rhodamine, 5 Å	107,000	4.09×10^{-16}	0.21	≈0.7	0.004
Ag, r = 60 nm	6.8×10^{10}	1.4×10^{-10}	5.0	0.55	1980.0
Au, r = 60 nm	5.3×10^{10}	6.3×10^{-11}	2.2	0.31	871.0
Qdots, r = 5 nm	1.8×10^{6}	7×10^{-15}	0.036	≈0.5	0.05
Polystyrene, r = 60 nm	5.8×10^{7}	2.2×10^{-13}	0.008	1.0	3.1